Title: Morphological and genetic divergence between two lineages of *Magnolia salicifolia* (Magnoliaceae) in Japan

Authors: Ichiro Tamaki [1], Naomichi Kawashima [2], Suzuki Setsuko [3], Akemi Itaya [4] and Nobuhiro Tomaru [2]

[1] Gifu Academy of Forest Science and Culture, Mino, Gifu 501-3714, Japan

[2] Graduate School of Bioagricultural Sciences, Nagoya University, Nagoya 464-8601, Japan

[3] Department of Forest Molecular Genetics and Biotechnology, Forestry and Forest Products Research Institute, Forest Research and Management Organization, Tsukuba, Ibaraki 305-8687, Japan

[4] Graduate School of Bioresources, Mie University, Tsu, Mie 514-8507, Japan

Corresponding author: Nobuhiro Tomaru

Graduate School of Bioagricultural Sciences, Nagoya University, Furo-cho, Chikusa-ku, Nagoya 464-8601, Japan

Tel: +81-52-789-4048; Fax: +81-52-789-5014;

E-mail: tomaru@agr.nagoya-u.ac.jp

Running title: Two diverged lineages in *Magnolia salicifolia*

ABSTRACT

Uncovering how populations of a species differ genetically and ecologically is important for understanding evolutionary processes. We investigated genetic structure using nuclear microsatellites and chloroplast DNA sequences and geographical variation in leaf morphological traits among *Magnolia salicifolia* populations across its entire species range. Two distinct lineages, northern and southern lineages, were genetically detected and both lineages had substructure among populations. The width/length ratio and area of leaves showed latitudinal gradients, while the position of the maximum leaf width exhibited a discontinuous change between the lineages. Approximate Bayesian computation detected exponential population growth and stable population size from the past to the present in the northern and southern lineages, respectively. Small amounts of migrations between the lineages were inferred. Divergence time between the lineages was estimated to be the early to middle Pleistocene. Ecological niche modeling showed single large potential distribution area on the Sea of Japan side and multiple intermittent ones on the Pacific Ocean side during the last glacial maximum.

We suggest that these distinct evolutionary histories of the northern and southern lineages after diversification have influenced not only neutral markers but also genes controlling leaf morphological traits.

ADDITONAL KEYWORDS: approximate Bayesian computation – chloroplast DNA – ecological niche modeling – genetic structure – intraspecific divergence – leaf morphological trait – nuclear microsatellite – phylogeography – population demography

INTRODUCTION

Although spatially heterogeneous distribution of morphological traits across populations along environmental gradients is considered to result mainly from natural selection associated with environmental factors, congruence may be observed between such morphological heterogeneity and genetic variation detected by neutral genetic markers. Several studies have reported such congruence within species (Butcher, McDonald & Bell, 2009; Hodgins & Barrett, 2007; Ikezaki *et al.*, 2016; Lagercrantz & Ryman, 1990; Pestano & Brown, 1999). This congruence can be due to circumstances in which population history influenced not only neutral genes but also the genes controlling morphological traits. Because migration counteracts natural selection, differentiation between morphological traits is rare between populations in which migration frequently occur, although it also depends on the strength of the selective pressure (Lenormand, 2002). When populations are isolated from each other for a long time and the level of migration is low, differentiation of not only neutral genes but also morphological traits affecting fitness can occur simultaneously (Pestano &

Brown, 1999). It is also known that even genes affecting fitness behave as though they are neutral when the product of effective population size and selective coefficient is low (Kimura, 1968). In other words, when populations are founded by a small number of individuals, traits affecting fitness can work like neutral genes.

Signatures of past population history (e.g. change in population size, divergence and admixture) can be observed in current genetic diversity within and among populations. A population that has experienced a severe bottleneck shows an excess of heterozygosity compared with that expected under mutation-drift equilibrium (Cornuet & Luikart, 1996), or, in the case of microsatellites, reductions in allele numbers relative to the overall range of allele sizes (Garza & Williamson, 2001). If there has been migration between diverged populations, individuals within these populations may show admixed multiple ancestries (Pritchard, Stephens & Donnelly, 2000). Such inferences based on summary statistics or model-based population structure analyses help us to understand past population history qualitatively but not quantitatively. However, population demographic modeling using coalescent theory or diffusion equation approximation based approaches

enable us to make quantitative inferences and moreover to compare different hypotheses (Csillery *et al.*, 2010; Excoffier *et al.*, 2013). Ecological niche modeling is another tool useful for inferring past population history. By applying a species distribution model, constructed using current distribution patterns and climate data, to paleoclimate data we can infer past potential distribution ranges. A combination of population demographic and ecological niche modelings may provide us with a deeper understanding of species history from multiple perspectives (Alvarado-Serrano & Knowles, 2014).

Probably because the Japanese archipelago is latitudinally long and there are environmental clines from south to north, gradients in leaf morphological traits in Japanese beech (*Fagus crenata*) along latitude have been reported (Hagiwara, 1977; Hashizume, Lee & Yamamoto, 1997). Moreover, climate conditions across the Japanese archipelago are different between the Sea of Japan and Pacific Ocean sides; the climate of this archipelago on the Sea of Japan side is characterized by heavy snowfall in winter. It is known that when related species are distributed on opposite sides, or when a single species is present on both sides, their life forms on

the Japan Sea differ from those on the Pacific Ocean sides (Fujita, 1987). For example, when pairs of deciduous tree varieties or species are compared, that distributed on the Sea of Japan side typically has broader, larger and thinner leaves than that on the Pacific Ocean side; this has been shown for between *Viburnum plicatum* var. *tomentosum* and *V. plicatum* var. *tomentosum* f. *glabrum*, between *Viburnum sieboldii* and *V. sieboldii* var. *obovatifolium*, between *Alnus serrulatoides* and *A. fauriei*, and between *Hamamelis japonica* and *H. japonica* var. *discolor*, where in each case the first of the pair is distributed on the Sea of Japan side (Hotta, 1974). Moreover, several studies have reported that species distributed across the entire Japanese archipelago show clear genetic structure (Hiraoka & Tomaru, 2009; Iwasaki *et al.*, 2012; Okaura *et al.*, 2007; Sakaguchi *et al.*, 2012).

Magnolia salicifolia (Siebold et Zucc.) Maxim. is a deciduous broad-leaved tree belonging to the Magnoliaceae which grows in warm-temperate and cool-temperate forests on the Honshu, Shikoku and Kyushu Islands of Japan (Fig. 1). Its habitat is mid slope or ridges and it likes relatively dry sites. *M. salicifolia* blooms in early spring and its flowers are insect pollinated. There are geographical variations in the

essential oils that are extracted from its flower buds, with two different types of oil in the populations distributed in northern Japan and another type found in those growing in southern Japan (Nagasawa *et al.*, 1969). Two ecotypes with different morphologies have been reported; a dwarf type with flowers with a high stamen/pistil in northern Japan, and a tree type whose flowers have a low stamen/pistil ratio in southern Japan (Takahashi, Shimoda & Hoshizaki, 2005). There are also differences in leaf morphology between the two types, with large, thin and wavy leaves on the dwarf type and small, thick and non-wavy leaves on the tree type, but these differences have not yet been examined in detail. Because of these characteristics, *M. salicifolia* is considered to be a suitable species in which to investigate the relationships between morphology and genetic structure and the effects of population history on morphology.

In this study, we investigated genetic structure among populations of *M. salicifolia* across its entire species range using nuclear microsatellites and chloroplast DNA (cpDNA) sequences. We also examined geographical variations in leaf morphological traits among the populations. To infer the past population history and potential distribution area of the species, we

performed, respectively, population demographic modeling using both nuclear microsatellites and cpDNA sequence data with the approximate Bayesian computation approach, and ecological niche modeling. Lastly, we addressed congruence between genetic structure and geographical variation in leaf morphological traits, and we discuss the effects of population history on morphological traits.

MATERIALS AND METHODS

Sample collection

We selected 24 populations from the entire distribution range of *M. salicifolia* and sampled 10 to 20 leaves per individual for DNA extraction and measurement of leaf morphology (Fig. 1 and Table 1). As *M. salicifolia* propagates asexually by natural layering, we sampled leaves only from trees standing more than 5 m apart from each other. The second or subsequent leaves from the top of a shoot, which were sufficiently expanded, were selected for morphological measurement. Since not enough leaves for

morphological measurement could be collected in population 5 (Tadami), samples from this population were used only for genetic analysis. We also sampled one individual of *M. denudata*, which was planted at Nagoya University (35.155N, 136.971E), as an outgroup for cpDNA sequence analysis. Leaves were transported to the laboratory in refrigerated conditions. After scanning leaf shape, leaves were stored at –30 ºC until required for DNA extraction.

DNA extraction, genotyping and sequencing

Total genomic DNA was extracted using a hexadecyltrimethylammonium bromide (CTAB) method (Murray & Thompson, 1980) with minor modification. Ten nuclear microsatellites (nSSRs) developed for *M. stellata*, which is a species related to *M. salicifolia*, stm0002, stm0163, stm0184, stm0214, stm0223, stm0246, stm0251, stm0415, stm0423 and stm0448 (Setsuko *et al.*, 2005), were amplified using a Multiplex PCR Kit (QIAGEN) with a GeneAmp PCR System 9700 (Applied Biosystems, Waltham, Massachusetts, USA) following the manufacturer's instructions. The amplified PCR products were electrophoresed with a 3100-Avant

Genetic Analyzer (Applied Biosystems). Microsatellite genotypes were then determined by GeneScan version 3.7 and Genotyper version 3.7 (Applied Biosystems).

Four non-coding cpDNA regions, *trnS–trnG* (Shaw *et al.*, 2005), *trnT–psbD* (Shaw *et al.*, 2007), *trnT–trnL* (Shaw *et al.*, 2005; Taberlet *et al.*, 1991) and *rpl36–infA–rps8–rpl14* (Shaw *et al.*, 2007), were sequenced from 2 to 4 individuals of each population of *M. salicifolia* and one individual of *M. denudata* (outgroup). The primers used in this study are listed in the Supporting Information, Table S1. The total volume for PCR was 5.0 μL, containing 1.0 μL of template DNA, 2.5 μL of AmpliTaq Gold Master Mix (Applied Biosystems) and 0.2 μM of each primer. The PCR was performed with an intial denaturation for 4 minutes at 94ºC followed by 30 cycles of denaturation for 1 minute at 94ºC, annealing for 1 minute at 55ºC and extension for 1 minute at 72ºC, with a final extension for 7 minutes at 72ºC. After precipitation of PCR products with polyethylene glycol, sequencing was performed directly by using a BigDye Terminator Cycle Sequencing Kit version 3.1 (Applied Biosystems) and the sequencing reaction products were electrophoresed on a 3130-Avant Genetic Analyzer (Applied

Biosystems).

Analysis of genetic diversity and differentiation

For each nSSR locus across all populations, the number of alleles (A), average gene diversity within populations (H_S), gene diversity in the total population (H_T) and Weir and Cockerham's F_{ST} were calculated. Hedrick's standardized G_{ST} [G'_{ST}; Hedrick (2005)] and Jost's D, which is another population differentiation measure (Jost, 2008), were also manually calculated. The significance of population differentiation at each locus was evaluated by a randomization test. For each population over all nSSR loci, allelic richness (A_R) based on nine diploid individuals, expected heterozygosity (H_E) and fixation index (F_{IS}) were calculated. The significance of departures from Hardy-Weinberg equilibrium at each locus was evaluated by a randomization test. Based on the two major genetic clusters detected by STRUCTURE analysis, we separated 24 populations into northern (populations 1 to 10) and southern (11 to 24) lineages (see details in "Genetic diversity and differentiation" in Results), and the differences in A_R, H_E and F_{IS} between the two lineages were evaluated by

randomization tests. The above calculations, apart from those of G'_{ST} and D were conducted using FSTAT version 2.9.3.2 (Goudet, 1995). We tested for the presence of an isolation by distance pattern, which indicates significant correlation between geographic and genetic distances, by the Mantel test with R package ade4 version 1.7.5 (Chessel, Dufour & Thioulouse, 2004). Kilometers on a log scale and $F_{ST}/(1-F_{ST})$ between population pairs were used as geographic and genetic distances, respectively. D_A distances between populations were calculated (Nei, Tajima & Tateno, 1983) and a neighbor-joining tree among populations based on these distances was then constructed, with R package ape version 4.0 (Paradis, Claude & Strimmer, 2004).

Genetic structure among populations was investigated with a model based clustering method implemented in STRUCTURE version 2.3.4 (Falush, Stephens & Pritchard, 2003; Pritchard, Stephens & Donnelly, 2000). The admixture and correlated allele frequency models were used. As suggested by Wang (2017), different α values for each genetic cluster were estimated and a low initial value of $\alpha = 0.05$ was applied. Different numbers of genetic clusters (K) from 1 to 22 were tested. For each K, the first 40,000

steps were discarded as a burn-in period and then 40,000 steps were used for the estimation of membership of each genetic cluster for each individual. The estimations of parameters were repeated 5 times for each *K*. To estimate the optimal *K*, the log probability of data and ΔK for each *K* were estimated with the R package corrsieve version 1.6.8 (Campana *et al.*, 2011; Evanno, Regnaut & Goudet, 2005). Analysis of molecular variance (AMOVA) was performed with Arlequin version 3.5.2 (Excoffier & Lischer, 2010). Genetic variation was hierarchically divided into three layers, which were the lineages inferred by STRUCTURE analysis, populations and individuals, and variance components for each layer and related Φ-statistics were calculated. The significance of each Φ-statistic was evaluated by a permutation test implemented in Arlequin.

CpDNA sequences were edited and assembled with DNA baser version 3 (Heracle BioSoft SRL), and then aligned with the MUSCLE algorithm in MEGA version 5.1 (Edgar, 2004; Tamura *et al.*, 2011). Mono- or di-nucleotide repeats in the sequences were omitted from subsequent analysis to avoid the possibility of homoplasy. CpDNA haplotypes were determined and a network among them was constructed using TCS version

1.21 (Clement, Posada & Crandall, 2000). The number of polymorphic sites (S), mean number of pairwise differences (π) and Tajima's D were calculated, and Tajima's test for selective neutrality (Tajima, 1989) was performed with Arlequin.

Analysis of variation in leaf morphology

Numerical conversion of leaf shape into elliptic Fourier descriptors and the measurement of leaf area were conducted with SHAPE version 1.3 (Iwata & Ukai, 2002). We used those principal components (PCs) the cumulative contribution of which to the total variance of data was more than 80%, which were obtained by SHAPE. Because that PC2 represented asymmetry of leaf shape, so that positive and negative values probably have no biological meaning, and since normality needed to be ensured, log-transformed absolute values of PC2 were used in the following analyses. Based on the PCs and leaf areas, nested-analysis of variance (ANOVA) was conducted to estimate variance components using R package lme4 version 1.1.12 (Bates *et al.*, 2015). Changes in PCs and leaf areas with latitude were assessed by using a generalized additive mixed-effect model (GAMM) in R

package gamm4 version 0.2.4 (Wood & Scheipl, 2016). Normal distribution and identity link were used, respectively, as error distribution and link function for the GAMM. Differences among individuals within populations and among populations were treated as random effects. *F*-tests were used to evaluate the significances of smooth terms.

Cluster analysis among the 24 populations using Ward's method based on Euclidian distances calculated from PCs (for PC2, log-transformed absolute values were also used) and leaf area was conducted with R package stats version 3.3.2 (R Core Team, 2016). All variables were standardized before calculating the distances.

Inference of population demography

To infer population demographic history in the two lineages inferred by STRUCTURE analysis, we employed a sequential approximate Bayesian computation (ABC) approach (Chen *et al.*, 2017). First, we applied population size change models for each lineage and then using the information from the results of these population size change models, we applied models of population divergence between the two lineages.

Four population size change models, which were the same except for the priors as those used in Chen *et al.* (2017), were built and were applied to each lineage (Fig. 2A). Model 1, a standard neutral model, assumes that there were no size changes in the past. Model 1 has one structural parameter, N_{CUR}, which is the current effective population size where a unit is the number of diploid individuals. Model 2, an exponential growth model, assumes that a population has grown exponentially from the past to the present according to the formula $N_T = N_{CUR} \times \exp(G \times T)$. N_T, G and T are, respectively, the effective population size at time T, growth rate and time from the present, where a unit is generation. A negative value of G indicates that the population has expanded from the past to the present. Model 2 thus has two structural parameters N_{CUR} and G. Model 3, an instantaneous size change model, assumes that the population size changed instantaneously at time T. Model 3 has three structural parameters, N_{CUR}, T and N_{ANC}. N_{ANC} is ancestral effective population size. Model 4, an exponential growth after instantaneous population size change model, is a combination of models 2 and 3. Model 4 has four structural parameters, N_{CUR}, G, T and N_{ANC}. The priors for all structural parameters are listed in the Supporting Information,

Table S2. The same priors were applied for all four models.

A generalized stepwise mutation model (GSM) was used as a model of mutation for nSSRs (Estoup, Jarne & Cornuet, 2002). GSM has two parameters, mutation rate per generation (μ) and a GSM geometric parameter (P_{GSM}). P_{GSM} ranges from 0 to 1 and represents the proportion of mutations that change allele sizes by more than one step; a value of zero means a strict stepwise mutation model (SMM). We simulated ten independent loci. The prior distribution for the mean value of μ among 10 loci was drawn from a log-uniform distribution from 10^{-5} to 10^{-3} (Supporting Information, Table S2) and each locus value of μ was randomly drawn from a gamma distribution with *shape* and *rate* parameters. The prior distribution of the *shape* parameter was drawn from a uniform distribution from 0.5 to 5 and the *rate* parameter was then calculated by *shape* / the mean value of μ. The prior distribution of the mean value of P_{GSM} among the 10 loci was drawn from a uniform distribution from 0 to 1 and each locus value of P_{GSM} was randomly drawn from a beta distribution with *a* and *b* parameters. The values of *a* and *b* were calculated from, respectively, 0.5 + 199 × the mean value of P_{GSM} and *a* × (1 – the mean value of P_{GSM}) /

the mean value of P_{GSM}, according to Excoffier, Estoup and Cornuet (2005). For cpDNA sequences, we simulated 3,929 bp sequences, which was the length of observed sequences excluding insertions/deletions (indels) and simple sequence repeats. The mutation rate for cpDNA sequences was set to 2.0×10^{-9} substitutions per site per generation (Muse, 2000; Sakaguchi *et al.*, 2012). Thus, all four models have three additional free parameters related to the mutation model, the mean value of μ, *shape* and the mean value of P_{GSM} for nSSR.

All priors were generated with R version 3.3.2 (R Core Team, 2016) and simulations were conducted with fastsimcoal2 version 2.5.2.21 (Excoffier & Foll, 2011). When simulating cpDNA sequences, the effective population size was set to half of that for nSSR because *M. salicifolia* is hermaphrodite and all individuals can become both maternal and paternal trees. Values of $2 \times N_{CUR}$ and N_{CUR}, representing the numbers of gene copies, were therefore passed to the coalescent simulator when simulating nSSR and cpDNA sequences, respectively. The simulations were repeated 5×10^5 times and summary statistics were calculated with arlsumstat version 3.5.2 (Excoffier & Lischer, 2010) for each model and for each lineage. The

average and standard deviation for the number of alleles, expected heterozygosity and allele size range were used as the summary statistics for nSSR. The number of polymorphic sites and the mean number of pairwise differences were used as the summary statistics for cpDNA sequences. Thus a total of eight summary statistics was used for the following analyses. The tolerance rate was set to 0.005 and 2,500 simulated data sets nearest to the observed data were used for model comparison and parameter estimation. The neural network regression method implemented in the R package abc version 2.1 was used for estimating posterior probabilities for models and posterior distribution for parameters (Csillery, Francois & Blum, 2012). Logit transformation of parameters was applied so as to keep the estimation of posterior distributions for parameters within prior ranges. The posterior mode and 95% highest posterior density (HPD) were calculated with density and HPDinterval functions of the R packages stats version 3.3.2 (R Core Team, 2016) and coda version 0.18 (Plummer *et al.*, 2006), respectively.

As models 2 and 1 were supported for the northern and southern lineages, respectively (see details in “Population demography” in Results), we assumed that the northern lineage had diverged from the southern

lineage in the past and subsequently expanded exponentially, while the southern lineage had kept its effective population size. Taking these assumptions into account, population divergence models were built (Fig. 2B). An isolation without migration model (I model) has four structural parameters, effective population size in the northern lineage (N_N), effective population size in the southern lineage (N_S), G and divergence time (T_{DIV}). An isolation with migration model (IM model) has six parameters including bidirectional migration rates, Nm_{NS} and Nm_{SN}, which are the number of migrants per generation from the northern to the southern lineages, and that from the southern to the northern lineages, respectively. Note that the direction of migration is toward coalescence, i.e. backward-in-time. When running simulations, Nm_{NS} and Nm_{SN} were divided by N_N and N_S, respectively, and the migration rates calculated were then passed to the coalescent simulator. In angiosperms, the migration rate revealed by the nuclear genome reflects both pollen and seed dispersal, while that of the chloroplast genome reflects only seed dispersal because the chloroplast genome is generally maternally-transmitted. When simulating cpDNA sequences, we thus multiplied migration rates by a coefficient β, which

ranges from 0 to 1, in order to allow for the reduction in migration rate for the chloroplast genome. The prior distribution of β was drawn from a uniform distribution from 0 to 1. To reduce computational costs and increase the accuracy of parameter estimation, G was fixed at -2.24×10^{-4} based on the results of the analysis of population size change models (see details in "Population demography" in Results). The prior distributions for other parameters, including mutation model parameters, are listed in the Supporting Information, Table S3.

The simulations in the population divergence models were repeated 1.5 million times in the same way as for the population size change models. However, when simulating nSSR data, only 200 individuals in each lineage were simulated, in order to reduce computational costs. Summary statistics were therefore calculated for 400 randomly selected individuals (200 individuals in each lineage). We also calculated F_{ST} for overall 10 nSSR loci and F_{ST} for cpDNA sequences to obtain additional summary statistics, and a total of 18 summary statistics was used for model comparison and parameter estimation. The tolerance value was set to 0.002 keeping the 3,000 simulated data sets that were closest to the observed data. Using these

datasets, model comparison and parameter estimation were also conducted in the same way as in the population size change models.

Finally, to evaluate the degree to which models fitted the observed data, posterior predictive simulations with 1,000 samples randomly drawn from the posterior distribution were conducted for both analyses of population size change and population divergence models. Summary statistics were calculated and compared to the corresponding observed data.

Ecological niche modeling

Ecological niche modeling was performed to infer the possible distribution ranges of *M. salicifolia* in the last glacial maximum (LGM; 21 kya) and last inter-glacial (LIG; 130 kya), using the maximum entropy method implemented in Maxent version 3.3.3k (Phillips, Anderson & Schapire, 2006). We used 176 location data points where the occurrence of *M. salicifolia* was recorded. These location data consisted of the 24 populations sampled in this study, our field observations and records from Global Biodiversity Information Facility (GBIF; http://www.gbif.org/). All records from GBIF were thoroughly checked against satellite images on Google

Maps (http://maps.google.com) and ambiguous or erroneous location data were removed. A current distribution model was constructed with six bioclimatic variables that took into account the ecological characteristics of the species: annual mean temperature (bio1), mean temperature of warmest quarter (bio10), mean temperature of coldest quarter (bio11), annual precipitation (bio12), precipitation in warmest quarter (bio18) and precipitation in coldest quarter (bio19) at a resolution of 2.5 arc-minutes; data were obtained from WorldClim (http://www.worldclim.com). Validation of the model was performed, using 100 replicates of cross-validation procedures, with 25% of the data for model testing, implemented in Maxent. Assuming uniformity of ecological niche for *M. salicifolia*, the model so constructed was applied to LGM and LIG climatic layers, which were also obtained from WorldClim, to predict distributions of the species in the past. The model for interdisciplinary research on climate [MIROC; Hasumi and Emori (2004)] and the community climate system model [CCSM; Collins *et al.* (2006)] were used to predict distributions during the LGM.

RESULTS

Genetic diversity and differentiation

The average values of the number of alleles (A) and average gene diversity within populations (H_S) over the 10 nuclear microsatellite loci across the 24 populations studied were 27.8 and 0.782, respectively (Supporting Information, Table S4). The values of F_{ST}, G'_{ST} and Jost's D over the 10 loci were 0.133, 0.613 and 0.556. All 10 loci showed significant population differentiation. Among the 24 populations over the 10 loci, allelic richness (A_R) based on nine individuals ranged from 4.43 to 10.31 with an average of 7.23 and expected heterozygosity (H_E) ranged from 0.605 to 0.905 with an average of 0.782 (Table 1). The population Ashu (15) showed the highest values of A_R and H_E. A_R and H_E in each population decreased continuously as distance from population 15 increased (Supporting Information, Figs. S1 and S2). Fixation index (F_{IS}) ranged from -0.138 to 0.149 within populations and its value over all populations was 0.064 (Table 1). Eleven of the 24 populations showed significant deviation from Hardy-Weinberg

disequilibrium.

The log probability of data in each K estimated by STRUCTURE analysis increased with increasing K and reached a plateau at K = 17 (Supporting Information, Fig. S3). Each genetic cluster at K = 17 corresponded well to one or two populations and most populations were dominated by single clusters. ΔK was highest at K = 2. The distribution of genetic clusters at K = 2 showed clear separation between northern and southern regions (Fig. 1). Clusters 1 and 2 dominated in the northern and southern regions, respectively. We therefore classified the 24 populations into northern (populations 1 to 10) and southern lineages (11 to 24). The value of F_{ST} between each cluster and the ancestral population was 3.63 times greater for cluster 1 (0.058) than for cluster 2 (0.016). The populations near the boundary between the two lineages, especially populations 9 and 15, showed genetic admixture between the two clusters. Although the difference in the average value of A_R between the two lineages was not significant, the average value of H_E was significantly lower in the northern lineage (0.735) than in the southern lineage (0.815, P = 0.012; Table 1).

Isolation by distance patterns were detected across all 24 populations

(R^2 = 0.347 and P < 0.001) and in both the northern and southern lineages (R^2 = 0.174, P = 0.004 and R^2 = 0.208, P < 0.001, respectively; Supporting Information, Fig. S4). The neighbor-joining tree based on D_A distances reflected geographical locations of populations well (Supporting Information, Fig. S5). Divergence between the northern and southern lineages was supported with a bootstrap probability of 87%.

The total length of aligned cpDNA sequences in four regions was 3,932 bp. Eleven substitutions and one indel were detected within the species and seven haplotypes were identified (Fig. 1 and Supporting Information, Table S5). All populations except for Kuraiyama (11) had single haplotypes. The populations in the northern lineage had only two haplotypes, while those in the southern lineage had six. The number of polymorphic sites (S) and mean number of pairwise differences (π) were much lower in the northern lineage (1 and 0.189) than in the southern lineage (10 and 3.349, respectively). A negative value of Tajima's D was detected in the northern lineage (-0.592), while a positive value was detected in the southern lineage (1.047). However, the results of Tajima's tests for selective neutrality were not significant for either lineage. All sequences for the eight haplotypes,

including one haplotype for the outgroup were deposited in the DDBJ/EMBL/GenBank database (LC222591–LC222622).

AMOVA was performed with three layers: between lineages, among populations within lineages and among individuals within populations (Table 2). Both nSSR and cpDNA haplotypes showed significant divergence between lineages with Φ_{CT} values of 0.053 and 0.195, respectively.

Variation in leaf morphology

Three principal components (PCs) detected by SHAPE made more than 80% cumulative contribution to the overall variance in PCs explaining the variation in leaf shape (Supporting Information, Table S6). PC1, PC2 and PC3 reflected, respectively, differences in leaf width/length ratios, curvature of the tip and base of a leaf, and position of the maximum leaf width (Fig. 3A). Significant differences in PC1, PC3 and leaf area between the northern and southern lineages were detected (Supporting Information, Table S7). Significant smooth terms along latitude were detected in PC1, PC3 and leaf area ($P < 0.001$; Figs. 3B, D and E), but not in PC2 ($P = 0.067$; Fig. 3C). The smooth terms in PC1 and leaf area acted linearly and there were

latitudinal clines in PC1 and leaf area, while that in PC3 acted non-linearly and the values for PC3 were higher in the southern lineage than in the northern lineage. The dendrogram constructed by cluster analysis showed a clear division between the northern and southern lineages, with the exception of population 3 (Yamabushidake; Fig. 3F). In summary, the northern lineage had wide leaves (large PC1), with the maximum width being near the central position (small PC3), and large leaf area, whereas the southern lineage had narrow leaves (small PC1), with their maximum width near the base (large PC3), and small leaf area (Fig. 3 and Supporting Information, Fig. S6).

Population demography

In the comparisons among four models of change in population size, the population expansion model (model 2) and standard neutral model (model 1) were best supported with probabilities of 0.574 and 0.503, for the northern and southern lineage, respectively (Table 3). Posterior predictive simulations for the best models for each lineage showed good fitting of the predicted values to the observed values (Supporting Information, Fig. S7).

In a comparison between the divergence models with or without migration, the isolation with migration model (IM model) was strongly supported, with a probability of 0.882 (Table 4). Posterior predictive simulations for the IM model showed good fitting of the predicted values to the observed values (Supporting Information, Fig. S8). All posterior distributions for the parameters in the IM model differed from their prior distributions and showed clear single peaks (Supporting Information, Fig. S9). Posterior modes (95% HPD) for effective population sizes in the northern (N_N) and southern lineage (N_S) were 254,000 (27,000–958,000) and 159,000 (44,000–404,000), respectively (Table 4). Although the mode of N_N was greater than that of N_S, the difference in posterior distribution was not significant with a posterior probability of 0.642. The posterior mode (95% HPD) for the divergence time between the two lineages (T_{DIV}) was 37,900 (12,200–970,600) generations ago. Effective population size in the northern lineage at time T_{DIV} was 52 (0.02% of the current size). The numbers of migrants per generation from the southern to the northern lineage (Nm_{NS}) and from the northern to the southern lineage (Nm_{SN}) in the forward-in-time direction were 0.97 (0.00–3.58) and 1.75 (0.00–8.84), respectively. Although the

mode of Nm_{SN} was greater than that of Nm_{NS}, the difference in posterior distribution was not significant with a posterior probability of 0.592. Posterior distributions for Nm_{NS} and Nm_{SN} were distributed around 1.0 (0.0 on the log scale in the Supporting Information, Fig. S9) and were not significantly different from 1.0.

Ecological niche modeling

Potential distribution maps for the present, LGM and LIG were created (Fig. 4). The accuracy of ecological niche modeling was high (the area under the curve = 0.987 and standard deviation = 0.002). The predicted distributions based on the present climatic data were well aligned with the species range (Figs. 1 and 4). The climate variable that made the greatest contribution to the total variance was precipitation in the coldest quarter (bio19, 41.3%).

The predicted distributions in the LGM based on MIROC and on CCSM showed similar patterns. There were large potential distribution areas on the Sea of Japan side of Honshu Island from 35ºN to 39ºN. On the Pacific Ocean side, intermittent potential distribution areas were detected in the southern parts of Honshu, Shikoku and Kyushu Islands. The area in the

southern part of Shikoku was the smallest among the three Islands. Although the predicted distributions in the LIG showed a pattern similar to the present, the area was larger in southern Japan and smaller in northern Japan.

DISCUSSION

Existence of two distinct lineages linked to leaf morphological differences

The results of STRUCTURE analysis gave two different estimates of optimal *K*s, 2 and 17. This indicates that there is hierarchical genetic structure. We therefore consider that there are two major lineages, the northern and southern lineages, which are subdivided into sets of populations. The neighbor-joining tree also supported the existence of the northern and southern lineages and within-lineage substructure. The northern and southern lineages correspond well with types I and II (northern Japan) and type III (southern Japan) of the essential oils extracted from flower buds (Nagasawa *et al.*, 1969) and with the dwarf (northern Japan)

and tree (southern Japan) types (Takahashi, Shimoda & Hoshizaki, 2005). Leaf morphological traits of *M. salicifolia* also clearly differed between the northern and southern lineages. Leaves of the northern lineage were wide, acute and large, while those of the southern one were narrow, acuminate and small.

Moreover, especially for PC1 and leaf area, clear latitudinal clines were detected. This indicates that leaves are wider and larger as latitude increases. Leaf morphological cline from south to north in Japanese beech (*Fagus crenata*), which is a dominant tree species in Japanese cool-temperate forests, has been reported (Hagiwara, 1977; Hashizume, Lee & Yamamoto, 1997). These studies showed that the leaves of Japanese beech were larger in area and had larger relative width with increasing latitude. These latitudinal trends in leaf morphology in Japanese beech are consistent with our observations on *M. salicifolia*. Differences in morphology between the northern and southern lineages of *M. salicifolia* may be based on genetic factors related to latitudinal changes in climate along the Japanese archipelago. However, effects of past population demography on these differences could not be ruled out, because historical demographic events

influence not only neutral genetic markers but also genes controlling traits related to fitness and consequently there can be concordance between morphological traits and genetic structure (Butcher, McDonald & Bell, 2009; Hodgins & Barrett, 2007; Lagercrantz & Ryman, 1990). Changes in PC3 showed no clear latitudinal cline; instead, they exhibited discontinuity. Changes in the position at which leaf width was maximum suggest that this trait may have been affected by not only effects of latitudinal environmental gradients but also effects of population history.

Different population demographic histories of the two lineages

According to the results of modeling changes in population size, the northern lineage had undergone exponential growth from the past to the present, whereas the southern one had a stable population size. The northern lineage consists mainly of the common haplotype A, while the southern one consists of all other haplotypes except for E. Haplotype G, which was detected in the southern lineage, is very distant from the common haplotype A. The genetic diversity of the southern lineage is clearly higher than that of the northern one; this applies to both genomes. The value of F_{ST} estimated

by STRUCTURE for cluster 2, which dominates in the southern lineage, was much lower than that for cluster 1, which dominates in the northern lineage, and this suggests that the effect of genetic drift is greater in the northern lineage than in the southern one. Taking all these findings into consideration, it appears that the northern lineage has diverged from the southern one and expanded from a small number of founders.

The time of divergence between the northern and southern lineages estimated by the IM model was 37,900 (12,200–970,600) generations ago. To convert this value into real time (years ago), a generation time (years per generation) must be assumed. Takahashi *et al.* (2006) reported that the flowering and fruiting ages of the dwarf type of *M. salicifolia* were 10.6±5.11 and 13.7±6.42 years, and those of the tree type were 17.6±6.57 and 20.4±6.70 years, respectively. The same authors also reported that the longevity of most dwarf type individuals was less than 50 years, while some tree type individuals survived for more than 100 years. With these data taken into consideration, we assumed that the average generation time of the two lineages was 30 years/generation and the divergence time in real units was thus inferred to be 1.14 (0.37–29.12) million years ago. It therefore

appears that the two lineages diverged in the early to middle Pleistocene and experienced several glacial-interglacial cycles after diversification.

Posterior modes of the number of migrants per generation (*Nm*) between lineages ranged from 0.97 to 1.75 and their posteriors were distributed around 1.0. Sewall Wright's famous one migrant per generation rule is that only one migrant per generation is enough to prevent complete population differentiation (Wright, 1931). However, this rule comes into effect under the ideal populations on the island model. In real populations, to prevent population differentiation, it has been reported that at least *Nm* = 1–10 is needed (Mills & Allendorf, 1996; Wang, 2004). Moreover, reported values of *Nm* among species or varieties of forest tree species calculated using the IM model were close to or higher than the value obtained in our study; for example, *Nm* = 8.79–10.11 among four *Quercus* species [calculated using the values shown in Table 4 of Leroy *et al.* (2017)], *Nm* = 1.78–5.84 between *Taxodium distichum* var. *distichum* and *T. distichum* var. *imbricarium* [calculated from the values shown in Table 6 of Ikezaki *et al.* (2016)] and 0.02–0.97 among three *Pinus* species [calculated using the values shown in the Supporting Information, Table S11 of Wachowiak,

Palme and Savolainen (2011)]. The *Nm* values for migration between the two lineages of *M. salicifolia* are low even by within–species standards and the extent of migration between them is relatively small. As migration counteracts natural selection (Lenormand, 2002), this low frequency of inter-lineage gene flow may have driven natural selection within each lineage and contributed to the different leaf shapes in the two lineages.

Ecological niche modeling detected a large continuous potential distribution area during LGM on the Sea of Japan side of central Honshu Island. This area is likely to have been the refugium of the northern and southern lineages during the LGM. The possibility is given further support by the high genetic diversity of populations in this area (especially populations 15 to 18) and in the finding that genetic diversity decreases with increasing distance from these populations. The potential distribution area on the Sea of Japan side of Honshu Island increased after the glacial period, especially toward the north. As the potential distribution area on the northern part of Honshu Island in LIG was small, the northern populations of the northern lineage probably settled after the last glacial period. This hypothesis is also supported by the dominance of haplotype A in the

northern populations of the northern lineage. The possibility of northward population expansion from this area has been pointed out by other publications on temperate forest tree species (Fujii *et al.*, 2002; Iwasaki *et al.*, 2012; Tomaru *et al.*, 1997). Potential distribution areas in LGM were also detected on the Pacific Ocean side. The southern part of Honshu Island near population 14, and southern Kyushu Island, may well have been additional refugia for the southern lineage, because there is a distinct haplotype D in population 14 and a distant haplotype G in Kyushu populations (populations 22–24) on its network. The potential distribution areas in the southern Japan during LIG were larger than those in the present. The existence of multiple refugia during glacial periods and large distribution areas during interglacial periods in southern Japan may have contributed to the high genetic diversity of the southern lineage with respect to both its nuclear and its chloroplast genome, and to the stability of its population size as inferred by ABC.

Conclusions

The analysis of genetic structure among populations using nuclear

microsatellites and cpDNA sequences clearly demonstrated that *M. salicifolia* consisted of two diverged lineages, the northern and southern lineages. Moreover, the analysis of leaf morphological traits revealed that the leaf width/length ratio, position of the maximum leaf width and leaf area were different between the two lineages and that the leaf width and area showed latitudinal clines, while the position of the maximum leaf width exhibited a discontinuous change between lineages. Based on the results from the genetic structure analysis, ABC and ecological niche modeling, it was inferred that the northern lineage expanded from a single refugium, present during the glacial period, starting from a small number of founders, whereas the southern lineage had multiple refugia and maintained a stable population size. Furthermore, the two lineages were inferred to have diverged in the early to middle Pleistocene and thereafter the level of migration between lineages may have been low, indicating that the two lineages have experienced multiple glacial-interglacial cycles in a condition of limited genetic connectivity between them. It is suggested that these distinct evolutionary histories of the northern and southern lineages after divergence have influenced not only neutral markers but also genes

controlling leaf morphological traits.

ACKNOWLEDGEMENTS

We thank Yoichi Watanabe of the Laboratory of Forest Ecology and Physiology of Nagoya University for his help in genetic and data analyses, and Shuhei Muranishi and other members of the Laboratory of Forest Ecology and Physiology of Nagoya University and Kazunori Takahashi of Forestry and Forest Products Research Institute for their assistance in sampling materials. We also thank anonymous reviewers for their helpful comments.

CONFLICT OF INTEREST

The authors declare no conflicts of interest.

DATA ARCHIVING

Chloroplast DNA sequences used in this study were deposited in the DDBJ/EMBL/GenBank data bases (LC222591–LC222622). Morphological and microsatellite data, and program scripts used in this study were deposited in the Dryad Digital Repository: http: (If the manuscript is accepted, we will submit there).

REFERENCES

Alvarado-Serrano DF, Knowles LL. 2014. Ecological niche models in phylogeographic studies: applications, advances and precautions. *Molecular Ecology Resources* **14:** 233–248.

Bates D, Maechler M, Bolker B, Walker S. 2015. Fitting linear mixed-effects models using lme4. *Journal of Statistical Software* **67:** 1–48.

Butcher PA, McDonald MW, Bell JC. 2009. Congruence between environmental parameters, morphology and genetic structure in Autrralia's most widely distributed eucalypt, *Eucalyptus camaldulensis*. *Tree Genetics & Genomes* **5:** 189–210.

Campana MG, Hunt HV, Jones H, White J. 2011. *Corrsieve*: software for summarizing and evaluating Structure output. *Molecular Ecology Resources* **11:** 349–352.

Chen C, Lu R, Zhu S, Tamaki I, Qiu Y. 2017. Population structure and historical demography of *Dipteronia dyeriana* (Sapindaceae), an extremely narrow palaeoendemic plant from China: implications for conservation in a biodiversity hotspot. *Heredity* **119:** 95–106.

Chessel D, Dufour AB, Thioulouse J. 2004. The ade4 package-I: One-table methods. *R News* **4:** 5–10.

Clement M, Posada D, Crandall K. 2000. TCS: a computer program to estimate gene genealogies. *Molecular Ecology* **9:** 1657–1660.

Collins WD, Bitz CM, Blackmon ML, Bonan GB, Bretherton CS, Carton JA, Chang P, Doney SC, Hack JJ, Henderson TB, Kiehl JT, Large WG, McKenna DS, Santer BD, Smith RD. 2006. The community climate system model version 3 (CCSM3). *Journal of Climate* **19:** 2122–2143.

Cornuet JM, Luikart G. 1996. Description and power analysis of two tests for detecting recent population bottlenecks from allele frequency data. *Genetics* **144:** 2001–2014.

Csillery K, Blum MGB, Gaggiotti OE, Francois O. 2010. Approximate Bayesian computation in practice. *Trends in Ecology and Evolution* **25:** 410–418.

Csillery K, Francois O, Blum MGB. 2012. abc: an R package for approximate Bayesian computation (ABC). *Methods in Ecology and Evolution* **3:** 475–479.

Edgar RC. 2004. MUSCLE: Multiple sequence alignment with high accuracy and high throughput. *Nucleic Acids Research* **32:** 1792–1797.

Estoup A, Jarne P, Cornuet J-M. 2002. Homoplasy and mutation model at microsatellite loci and their consequences for population genetics analysis. *Molecular Ecology* **11:** 1591–1604.

Evanno G, Regnaut S, Goudet J. 2005. Detecting the number of clusters of individuals using the software STRUCTURE: a simulation study. *Molecular Ecology* **14:** 2611–2620.

Excoffier L, Dupanloup I, Huerta-Sanchez E, Sousa VC, Foll M. 2013. Robust demographic inference from genomic and SNP data. *PLoS Genetics* **9:** e1003905.

Excoffier L, Estoup A, Cornuet J-M. 2005. Bayesian analysis of an admixture model with mutations and arbitrarily linked markers. *Genetics* **169:** 1727–1738.

Excoffier L, Foll M. 2011. fastsimcoal: a continuous-time coalescent simulator of genomic diversity under arbitrarily complex scenarios. *Bioinfomatics* **27:** 1332–1334.

Excoffier L, Lischer HE. 2010. Arlquin suite ver 3.5: a new series of programs to perform population genetics analyses under Linux and Windows. *Molecular Ecology Resources* **10:** 564–567.

Falush D, Stephens M, Pritchard JK. 2003. Inference of population structure using multilocus genotype data: linked loci and correlated allele frequencies. *Genetics* **164:** 1567–1587.

Fujii N, Tomaru N, Okuyama K, Koike T, Mikami T, Ueda K. 2002. Chloroplast DNA phylogeography of *Fagus crenata* (Fagaceae) in Japan. *Plant Systematics and Evolution* **232:** 21–33.

Fujita N. 1987. One-sided distribution of the component species of the Japanese beech forest along either the Pacific or the Japan Sea. *Acta Phytotaxonomica et Geobotanica* **38:** 311–329 (in Japanese with English abstruct).

Garza JC, Williamson EG. 2001. Detection of reduction in population size using data from microsatellite loci. *Molecular Ecology* **10:** 305–318.

Goudet J. 1995. FSTAT (version 1.2): a computer program to calculate *F*-statistics. *Journal of Heredity* **86:** 485–486.

Hagiwara S. 1977. Clines on leaf size of beech *Fagus crenata*. *Species Biological Research* **1:** 39–51 (in Japanese).

Hashizume H, Lee NH, Yamamoto F. 1997. Variation in the leaf shape of planted trees of *Fagus crenata* Blume among provinances. *Applied Forest Science* **6:** 115–118 (in Japanese with English abstract).

Hasumi H, Emori S. 2004. *K-1 Coupled GCM (MIROC) Description*. Center for Climate System Research, University Tokyo, National Institute for Environmental Studies, Frontier Research Center for Global Change: Tokyo Japan.

Hedrick PW. 2005. A standardized genetic differentiation measure. *Evolution* **59:** 1633–1638.

Hiraoka K, Tomaru N. 2009. Genetic divergence in nuclear genomes between populations of *Fagus crenata* along the Japan Sea and Pacific sides of Japan. *Journal of Plant Research* **122:** 269–282.

Hodgins KA, Barrett SCH. 2007. Population structure and genetic diversity in tristylous *Narcissus triandrus*: insights from microsatellites and chloroplast DNA variation. *Molecular Ecology* **16:** 2317–2332.

Hotta M. 1974. *Evolutionary biology in plants III: history and geography of plants*. Sanseido: Tokyo, Japan (in Japanese).

Ikezaki Y, Suyama Y, Middleton BA, Tsumura Y, Teshima K, Tachida H, Kusumi J. 2016. Inference of population structure and demographic history for *Taxodium distichum*, a coniferous tree in North America, based on amplicon sequencing analysis. *American Journal of Botany* **103:** 1937–1949.

Iwasaki T, Aoki K, Seo A, Murakami N. 2012. Comparative phylogeography of four component species of deciduous broad-leaved forests in Japan based on chloroplast DNA variation. *Journal of Plant Research* **125:** 207–221.

Iwata H, Ukai Y. 2002. SHAPE: A computer program package for quantitatibe evaluation of biological shapes based on elliptic Fourier descriptors. *Journal of Heredity* **93:** 384–385.

Jost L. 2008. G_{ST} and its relatives do not measure differentiation. *Molecular Ecology* **17:** 4015–4026.

Kimura M. 1968. Genetic variability maintained in a finite population due to mutational production of neutral and nearly neutral isoalleles. *Genetics Research* **11:** 247–269.

Lagercrantz U, Ryman N. 1990. Genetic structure of norway spruce (*Picea abies*): concordance of morphological and allozymic variation. *Evolution* **44:** 38–53.

Lenormand T. 2002. Gene flow and the limits to natural selection. *Trends in Ecology and Evolution* **17:** 183–189.

Leroy T, Roux C, Villate L, Bodenes C, Romiguier J, Paiva JAP, Dossat C, Aury J-M, Plomion C, Kremer A. 2017. Extensive recent secondary contacts between four European white oak species. *New Phytologist* **214:** 865–878.

Mills LS, Allendorf FW. 1996. The one-migrant-per-generation rule in conservation and management. *COnservation Biology* **10:** 1509-1518.

Murray MG, Thompson WF. 1980. Rapid isolation of high molecular weight plant DNA. *Nucleic Acids Research* **8:** 4321–4326.

Muse SV. 2000. Examining rates and patterns of nucleotide substitution in plants. *Plant Molecular Biology* **42:** 25–43.

Nagasawa M, Murakami T, Ikeda K, Hisada Y. 1969. The geographical variation of essential oils of Flos Magnoliae. *Yakugaku Zasshi* **89:** 454–459.

Nei M, Tajima F, Tateno Y. 1983. Accuracy of estimated phylogenetic trees from molecular data. *Journal of Molecular Evolution* **19:** 153-170.

Okaura T, Quang ND, Ubukata M, Harada K. 2007. Phylogeographic structure and late Quaternary population history of the Japanese oak *Quercus mongolica* var. *crispula* and related species revealed by chloroplast DNA variation. *Genes and Genetic Systems* **82:** 465-477.

Paradis E, Claude J, Strimmer K. 2004. Ape: analyses of phylogenetics and evolution in R language. *Bioinfomatics* **20:** 289-290.

Pestano J, Brown RP. 1999. Geographical structuring of mitochondrial DNA in *Chalcides sexlineatus* within the island of Gran Canaria. *Proceedings of the Royal Society B* **266:** 805−812.

Phillips SJ, Anderson RP, Schapire RE. 2006. Maximum entropy modeling of species geographic distributions. *Ecological Modelling* **190:** 231–259.

Plummer M, Best N, Cowles K, Vines K. 2006. CODA: Convergence Diagnosis and Output Analysis for MCMC. *R News* **6:** 7–11.

Pritchard JK, Stephens M, Donnelly P. 2000. Inference of population structure using multilocus genotype data. *Genetics* **155:** 945-959.

R Core Team. 2016. *R: a language and environment for statistical computing*. R Foundation for Statistical Computing: Vienna, Austria.

Sakaguchi S, Qiu Y-X, Liu Y-H, Qi X-S, Kim S-H, Han J, Takeuchi Y, Worth JRP, Yamasaki M, Sakurai S, Isagi Y. 2012. Climate oscillation during the Quaternary associated with landscape heterogeneity promoted allopatric lineage divergence of a temperate tree *Kalopanax septemlobus* (Araliaceae) in East Asia. *Molecular Ecology* **21:** 3823–3838.

Setsuko S, Ueno S, Tsumura Y, Tomaru N. 2005. Development of microsatellite markers in *Magnolia stellata* (Magnoliaceae), a threatened Japanese tree. *Conservation Genetics* **6:** 317–320.

Shaw J, Lickey EB, Beck JT, Farmer SB, Liu W, Miller J, Siripun KC, Winder CT, Schilling EE, Small RL. 2005. The tortoise and the hare II: relative utility of 21 noncoding chloroplast DNA sequences for phylogenetic analysis. *American Journal of Botany* **92:** 142-166.

Shaw J, Lickey EB, Schilling EE, Small RL. 2007. Comparison of whole chloroplast genome sequences to choose noncoding regions for phylogenetic studies in angiosperms: the tortoise and the hare III. *American Journal of Botany* **94:** 275-288.

Taberlet P, Gielly L, Pautou G, Bouvet J. 1991. Universal primers for amplification of three non-coding regions of chloroplast DNA. *Plant Molecular Biology* **17:** 1105–1109.

Tajima F. 1989. Statistical method for testing the neutral mutation hypothesis by DNA polymorphism. *Genetics* **123:** 585–595.

Takahashi K, Hoshizaki K, Masaki T, Osumi K. 2006. Comparative analysis of size structure and life span between *Magnolia salicifolia* and the dwarf sub-species newly found. *Kanto Journal of Forest Research* **57:** 113–114 (in Japanese).

Takahashi K, Shimoda N, Hoshizaki K. 2005. Botanical characteristics and distribution for a newly found sub-species of *Magnolia salicifolia* (Maxim.) Sieb. & Zucc. *Kanto Journal of Forest Research* **56:** 211–212 (in Japanese).

Tamura K, Peterson D, Peterson N, Stecher G, Nei M, Kumar S. 2011. MEGA5: Molecular evolutionary genetic analysis using maximum likelihood, evolutionary distance, and maximum parsimony methods. *Molecular Biology and Evolution* **28:** 2731–2739.

Tomaru N, Mitsutsuji T, Takahashi M, Tsumura Y, Uchida K, Ohba K. 1997. Genetic diversity in *Fagus crenata* (japanese beech): influence of the distributional shift during the late-Quaternary. *Heredity* **78:** 241–251.

Wachowiak W, Palme AE, Savolainen O. 2011. Speciation history of three closely related pines *Pinus mugo* (T.), *P. uliginosa* (N.) and *P. sylvestris* (L.). *Molecular Ecology* **20:** 1729–1743.

Wang J. 2004. Application of the one-migrant-per-generation rule to conservation and management. *COnservation Biology* **18:** 332–343.

Wang J. 2017. The computer program STRUCTURE for assigning individuals to populations: easy to use but easier to misuse. *Molecular Ecology Resources* **17:** 981–990.

Wood S, Scheipl F. 2016. gamm4: Generalized Additive Mixed Model using ‘mgcv’ and ‘lme4’. R package version 0.2-4. <https://CRAN.R-project.org/package=gamm4> Accessed June 27, 2017.

Wright S. 1931. Evolution in Mendelian populations. *Genetics* **16:** 97–159.

Titles and legends to figures

Figure 1. The locations of the 24 populations studied and the distributions of genetic clusters at $K = 2$ detected by STRUCTURE analysis and chloroplast DNA haplotypes across the distribution range (gray area) of *Magnolia salicifolia*, with a network of the haplotypes. Numbers indicates the population numbers as listed in Table 1. Pie charts and bold letters indicate, respectively, the proportions of genetic clusters at $K = 2$ and the haplotypes detected within populations. F_{ST} for each cluster indicates the extent of genetic divergence from the ancestral population. *N* indicates the number of individuals having each haplotype.

Figure 2. Population size change models (A) and population divergence models (B) applied to the northern and southern lineages of *Magnolia salicifolia*. For the population size change models, model 1, standard neutral model; model 2, exponential growth model; model 3, instantaneous size change model; model 4, exponential growth after instantaneous size change model. N_{CUR}, current effective population size, where the unit is the number

of diploid individuals; G, growth rate [N_T / N_{CUR} = exp ($G \times T$), where N_T is the effective population size at time T]; T, time when the population size changed. For the population divergence models, I model, isolation without migration model; IM model, isolation with migration model. N_N and N_S, current effective population sizes in the northern and southern lineages, respectively; G, growth rate; T_{DIV}, divergence time between northern and southern lineages; Nm_{NS} and Nm_{SN}, number of migrants per generation from the northern to the southern lineage and from the southern to the northern lineage, respectively. The direction of migration is toward coalescence, i.e., backward-in-time. All time parameters are in units of generations.

Figure 3. Changes in leaf shape between -2 SD, average and +2 SD values of the three principal components (PCs), estimated by elliptic Fourier descriptors with SHAPE, which made more than 80% cumulative contribution to the overall variance explaining the variation in leaf shape in *Magnolia salicifolia* (A). SD indicates standard deviation. Changes in three PCs (B–D) and leaf area (E) against latitude across the 23 populations. White and black circles indicate populations in the northern and southern

lineage, respectively. Lines and gray areas indicate, respectively, the maximum likelihood estimates (MLEs) and 95% confidence intervals inferred by the generalized additive mixed-effect model. When the smooth term was not significant, MLE is not shown. Dendrogram of the 23 populations from cluster analysis using Ward's method based on Euclidian distances calculated with PC1, log (|PC2|), PC3 and leaf area (F).

Figure 4. Inferred potential distribution areas for *Magnolia salicifolia* in the present, the last inter-glacial (LIG; 130 kya) and the last glacial maximum (LGM; 21 kya) based on the model for interdisciplinary research on climate (MIROC) and the community climate system model (CCSM). *P* indicates probability of occurrence. Circles and plus symbols indicate, respectively, the 24 populations sampled and records of occurrences used for the model construction.

SUPPORTING INFORMATION

Additional Supporting Information may be found in the online version of this article at the publisher's web site:

Table S1. The four non-coding chloroplast DNA regions that were sequenced in this study.

Table S2. Prior distributions in the population size change models.

Table S3. Prior distributions in the population divergence models.

Table S4. Genetic diversity at 10 nuclear microsatellite loci across the 24 populations of *Magnolia salicifolia* studied.

Table S5. Nucleotide sequence variation among seven haplotypes in four chloroplast DNA regions of *Magnolia salicifolia* and *M. denudata* (outgroup).

Table S6. Three principal components (PCs) explaining the variation in leaf shape.

Table S7. Hierarchically estimated variance components for three principal components (PCs) explaining the variation in leaf shape and leaf area.

Figure S1. Distributions of genetic diversity in the 24 populations of *Magnolia salicifolia*.

Figure S2. Latitudinal and longitudinal changes in allelic richness based on nine individuals and expected heterozygosity calculated from 10 nuclear microsatellite loci in the 24 populations of *Magnolia salicifolia*.

Figure S3. Results from STRUCTURE analysis.

Figure S4. Geographic distance (km) transformed to natural logarithms and genetic distances [$F_{ST}/(1-F_{ST})$] estimated with 10 nuclear microsatellite loci for all 24, the northern 10 and the southern 14 populations of *Magnolia salicifolia*.

Figure S5. Neighbor-joining tree constructed based on D_A distances estimated with 10 nuclear microsatellite loci among the 24 populations of *Magnolia salicifolia*.

Figure S6. Distributions for PC1, PC2, PC3 and leaf area across 23 populations of *Magnolia salicifolia*.

Figure S7. Results from the posterior predictive simulations in models 2 and 1 of the population size change models for the northern and southern lineages of *Magnolia salicifolia*.

Figure S8. Results from the posterior predictive simulations for the isolation with migration model (IM model) of the population divergence models in the northern and southern lineages of *Magnolia salicifolia*.

Figure S9. Prior and posterior distributions for the isolation (I) model and isolation with migration (IM) models in the northern and southern lineages of *Magnolia salicifolia*.

Table 1. Location, sample size and population genetic statistics for the 24 populations of *Magnolia salicifolia* studied

Population											
No.	Name	Latitude	Longitude	Lineage [a]	N_n	N_c	N_m	A_R	H_E	F_{IS} [b]	
1	Hakkodasan	40.65	140.90	Northern	31	2	33	4.43	0.605	0.010	N.S.
2	Taiheizan	39.78	140.22	Northern	32	2	32	5.66	0.702	0.145	**
3	Yamabushidake	38.97	140.58	Northern	31	2	31	7.00	0.744	0.062	N.S.
4	Gassan	38.55	140.02	Northern	32	2	32	5.24	0.645	0.026	N.S.
5	Tadami	37.40	139.35	Northern	30	2	–	8.12	0.830	0.129	**
6	Sumondake	37.28	139.13	Northern	28	2	30	7.17	0.772	0.102	*
7	Nonomiike	37.02	138.52	Northern	9	2	24	7.20	0.746	0.061	N.S.
8	Amakazariyama	36.90	137.97	Northern	38	2	37	7.24	0.749	0.081	*
9	Komatsu	36.32	136.44	Northern	29	2	30	7.53	0.798	0.086	*
10	Hida	36.23	136.95	Northern	30	2	34	7.70	0.760	0.149	**
11	Kuraiyama	35.99	137.21	Southern	24	4	32	6.47	0.756	0.104	*
12	Mennoki	35.18	137.53	Southern	30	2	30	5.81	0.725	-0.138	N.S.
13	Gozaishodake	35.02	136.43	Southern	32	2	33	8.90	0.871	0.043	N.S.
14	Odaigahara	34.18	136.10	Southern	11	2	12	8.21	0.838	0.040	N.S.
15	Ashu	35.30	135.72	Southern	32	2	32	10.31	0.905	0.059	*
16	Hyonosen	35.35	134.52	Southern	32	2	32	9.45	0.897	0.022	N.S.
17	Daisen	35.38	133.53	Southern	30	2	30	8.62	0.877	0.117	**
18	Kotobikisan	35.03	132.80	Southern	32	2	32	9.34	0.878	0.065	*
19	Tsurugisan	33.88	134.12	Southern	32	2	32	7.91	0.858	0.049	N.S.
20	Shiragayama	33.82	133.58	Southern	24	2	24	7.53	0.831	0.029	N.S.
21	Ishizuchiyama	33.75	133.07	Southern	31	2	31	6.91	0.800	-0.008	N.S.
22	Soeda	33.53	130.85	Southern	27	2	27	5.88	0.746	0.078	N.S.
23	Kinryusan	33.35	130.30	Southern	30	2	30	5.73	0.737	0.148	**
24	Shiba	32.37	131.15	Southern	30	2	30	5.21	0.692	0.069	N.S.
Average / overall											
	Northern				29.0	2.0	31.4	6.73	0.735	0.088	
	Southern				28.4	2.1	29.1	7.59	0.815	0.045	
	All				28.6	2.1	30.0	7.23	0.782	0.064	

N_n, number of individuals for analysis of nuclear microsatellites; N_c, number of individuals for analysis of chloroplast DNA sequences; N_m, number of individuals for analysis of leaf morphology; A_R, allelic richness based on nine diploid individuals; H_E, expected heterozygosity; F_{IS}, fixation index.

[a] Lineages were determined by STRUCTURE analysis.

[b] The significance of departures from Hardy-Weinberg equilibrium was tested by randomization tests. *P*-values were adjusted with Bonferroni correction. N.S., not significant; *, $P < 0.05$; **, $P < 0.01$.

Table 2. Results from analysis of molecular variance for nuclear microsatellites and chloroplast DNA haplotypes

	Nuclear microsatellite			Chloroplast DNA haplotype		
Layer	Variance component (%)	Φ–statistics		Variance component (%)	Φ–statistics	
Between lineages	5.3	$\Phi_{CT} = 0.053$	***	19.5	$\Phi_{CT} = 0.195$	***
Among populations within lineages	10.3	$\Phi_{SC} = 0.109$	***	78.6	$\Phi_{SC} = 0.976$	***
Among individuals within populations	84.4	$\Phi_{ST} = 0.156$	***	1.9	$\Phi_{ST} = 0.981$	***

***, $P < 0.001$.

Table 3. Posterior model probabilities, and posterior modes and 95% highest posterior densities (HPDs) for parameters in the models of population size change, for the northern and southern lineages of *Magnolia salicifolia*

			Parameter (mode / 95% HPD)						
Lineage	Model	Posterior probability	N_{CUR} ($\times 10^5$)	G ($\times 10^{-4}$)	T	N_{ANC} ($\times 10^5$)	mean μ for nSSR ($\times 10^{-4}$)	*shape*	mean P_{GSM}
Northern	Model 1	0.040	0.28 (0.04–1.00)				7.14 (0.82–10.00)	0.83 (0.50–2.52)	0.45 (0.26–0.57)
	Model 2	**0.574**	**1.01 (0.17–7.07)**	**-2.24 (-9.13–-0.47)**			**5.18 (1.26–9.98)**	**0.82 (0.50–2.51)**	**0.46 (0.35–0.60)**
	Model 3	0.158	1.64 (0.10–9.94)		777 (15–65396)	0.10 (0.01–0.61)	2.68 (0.67–9.99)	0.88 (0.50–2.52)	0.47 (0.28–0.59)
	Model 4	0.228	0.94 (0.10–9.98)	-3.73 (-9.82–-0.52)	30973 (14–99433)	0.19 (0.02–7.21)	5.28 (1.09–10.00)	0.86 (0.50–2.38)	0.43 (0.27–0.57)
Southern	**Model 1**	**0.503**	**1.55 (0.60–3.50)**				**0.93 (0.27–3.44)**	**2.79 (1.15–4.89)**	**0.28 (0.01–0.50)**
	Model 2	0.010	1.44 (0.46–6.39)	-0.04 (-0.42–0.00)			0.71 (0.19–3.85)	2.28 (1.04–4.98)	0.32 (0.01–0.59)
	Model 3	0.270	2.60 (0.03–10.00)		7 (1–37191)	1.36 (0.49–3.59)	0.73 (0.24–3.59)	2.71 (1.11–4.94)	0.24 (0.02–0.44)
	Model 4	0.217	3.56 (0.03–9.99)	-1.47 (-9.50–-0.01)	6 (1–1902)	1.25 (0.55–4.54)	0.95 (0.27–4.56)	2.81 (1.05–4.95)	0.23 (0.01–0.42)

The best supported model is shown in bold type. Model 1, standard neutral model; model 2, exponential growth model; model 3, instantaneous size change model; model 4, exponential growth after instantaneous size change model. N_{CUR}, current effective population size, where the unit is number of diploid individuals; G, growth rate [N_T / N_{CUR} = exp ($G \times T$), where N_T is the effective population size at time T]; T, time when the population size changed; μ, average mutation rate among nSSR loci; *shape*, parameter for gamma distribution related to the variation in mutation rate at each locus; P_{GSM}, parameter for the generalized stepwise mutation model (GSM), representing the proportion of mutations that changes allele sizes by more than one step. All time parameters are in units of generations.

Table 4. Posterior model probabilities, and posterior modes and 95% highest posterior densities (HPDs) for the parameters, in the models of population divergence, for the northern and southern lineages of *Magnolia salicifolia*

	Model (mode / 95% HPD)	
	I model	**IM model**
Posterior probability	0.119	**0.882**
Number of free parameters	6	**9**
Parameter		
N_N ($\times 10^5$)	3.24	**2.54**
	(0.55–9.98)	**(0.27–9.58)**
N_S ($\times 10^5$)	1.40	**1.59**
	(0.50–3.47)	**(0.44–4.04)**
T_{DIV} ($\times 10^4$)	0.99	**3.79**
	(0.43–6.47)	**(1.22–97.06)**
Nm_{NS}	—	**0.97**
	—	**(0.00–3.58)**
Nm_{SN}	—	**1.75**
	—	**(0.00–8.84)**
β	—	**0.22**
	—	**(0.02–0.96)**
mean μ for nSSR ($\times 10^{-4}$)	1.57	**2.77**
	(0.41–8.00)	**(0.98–9.98)**
shape	0.81	**0.94**
	(0.50–3.31)	**(0.51–3.51)**
mean P_{GSM}	0.24	**0.25**
	(0.02–0.55)	**(0.03–0.46)**

The best supported model is shown in bold type. I model, isolation without migration model; IM model, isolation with migration model. N_N and N_S, current effective population sizes in the northern and southern lineages, respectively, where the unit is the number of diploid individuals; T_{DIV}, divergence time (generation) between northern and southern lineages; Nm_{NS} and Nm_{SN}, number of migrants per generation from the northern to the southern lineage and from the southern to the northern lineage, respectively (the direction of migration is toward coalescence, i.e., backward-in-time); β, reduction in the migration rate for chloroplast DNA; μ, average mutation rate among nSSR loci; *shape*, parameter for gamma distribution related to the variation in mutation rates at each locus; P_{GSM}, parameter for the generalized stepwise mutation model (GSM), representing the proportion of mutations that changes allele sizes by more than one step.

Fig. 1

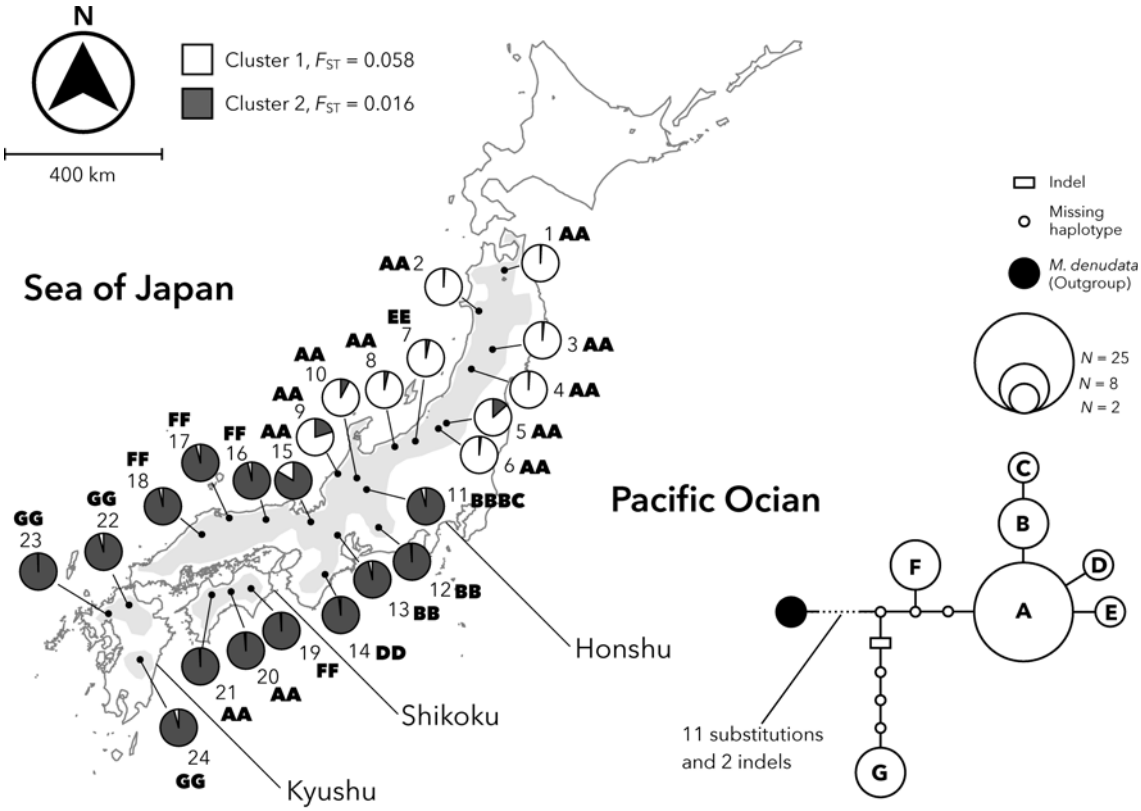
N
400 km
Cluster 1, F_{ST} = 0.058
Cluster 2, F_{ST} = 0.016
Sea of Japan
Pacific Ocian
Honshu
Shikoku
Kyushu
1 AA
2 AA
3 AA
4 AA
5 AA
6 AA
7 EE
8 AA
9 AA
10 AA
11 BBBC
12 BB
13 BB
14 DD
15 AA
16 FF
17 FF
18 FF
19 FF
20 AA
21 AA
22 GG
23 GG
24 GG
Indel
Missing haplotype
M. denudata (Outgroup)
N = 25
N = 8
N = 2
A
B
C
D
E
F
G
11 substitutions and 2 indels

Fig. 2

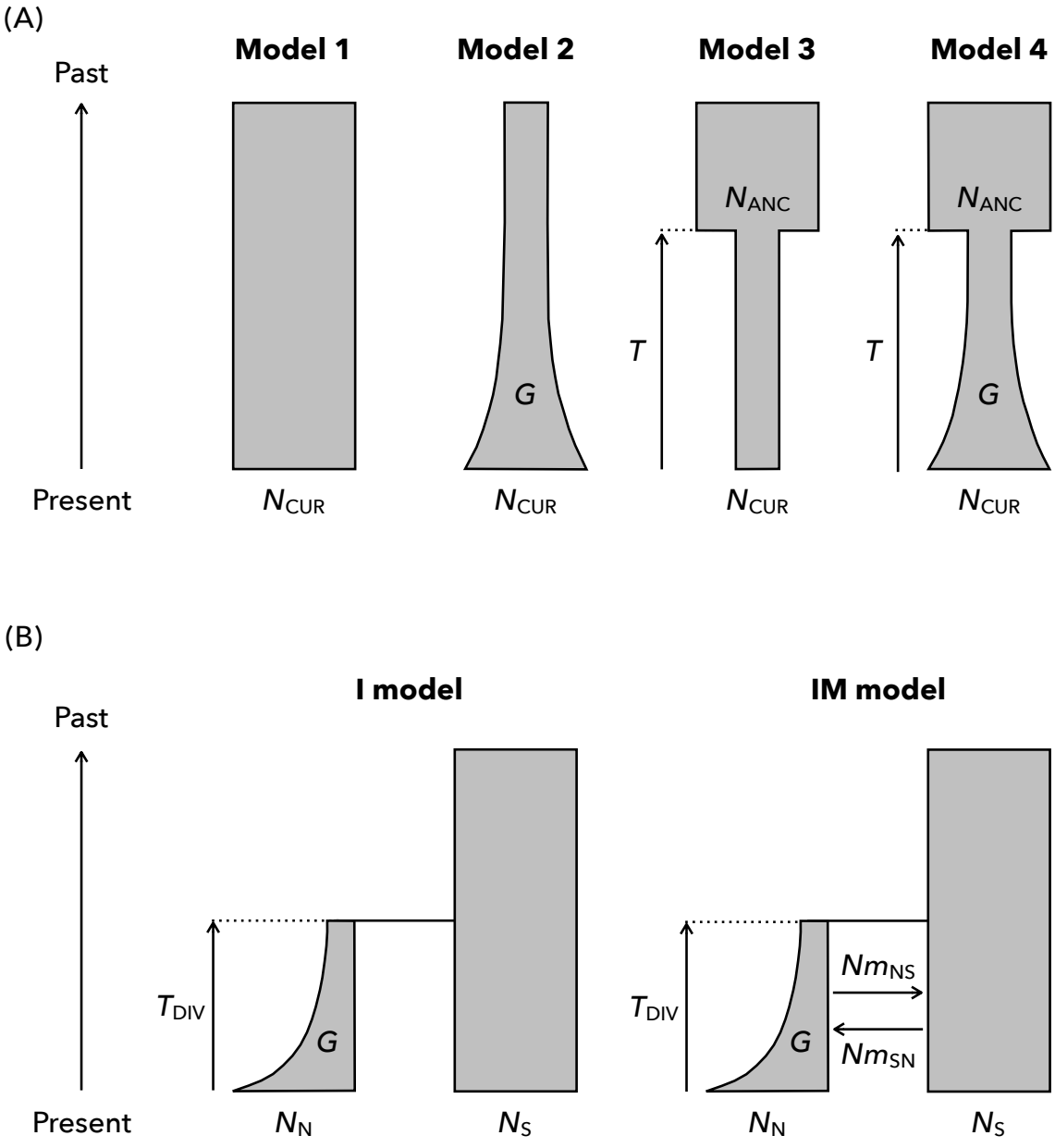
(A)
Model 1
Model 2
Model 3
Model 4
Past
Present
N_{ANC}
T
G
N_{CUR}
(B)
I model
IM model
T_{DIV}
Nm_{NS}
Nm_{SN}
N_N
N_S

Fig. 3

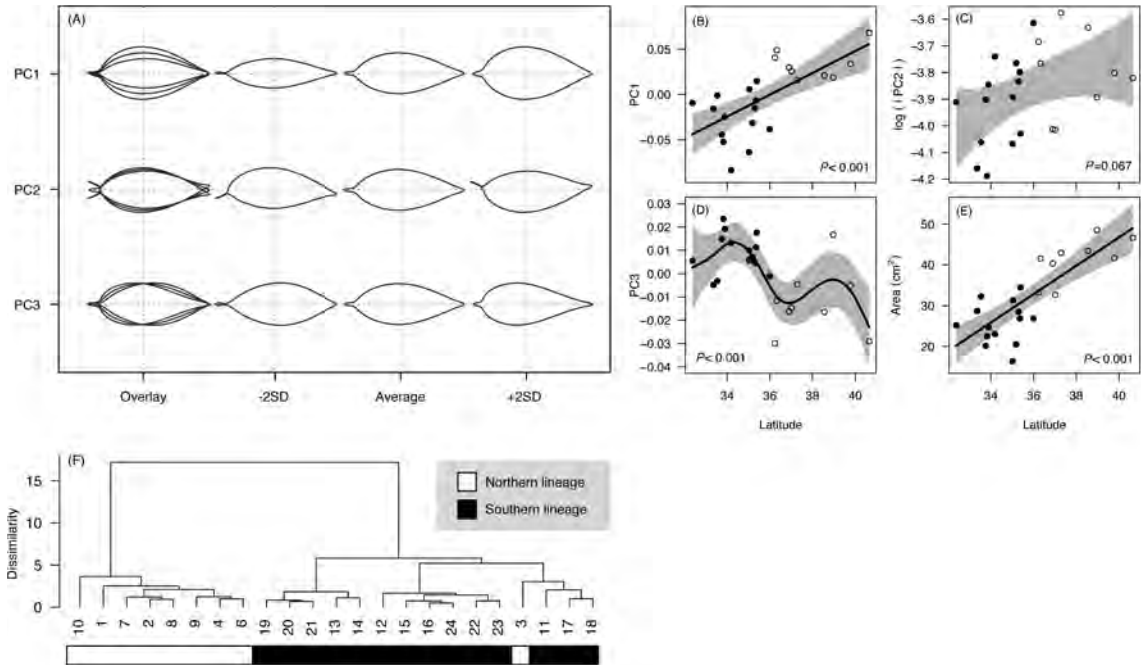
(A)
PC1
PC2
PC3
Overlay
-2SD
Average
+2SD
(B)
PC1
P< 0.001
(C)
log (| PC2 |)
P=0.067
(D)
PC3
P< 0.001
(E)
Area (cm²)
P< 0.001
Latitude
Latitude
(F)
Dissimilarity
Northern lineage
Southern lineage
10 1 7 2 8 9 4 6 19 20 21 13 14 12 15 16 24 22 23 3 11 17 18

Fig. 4

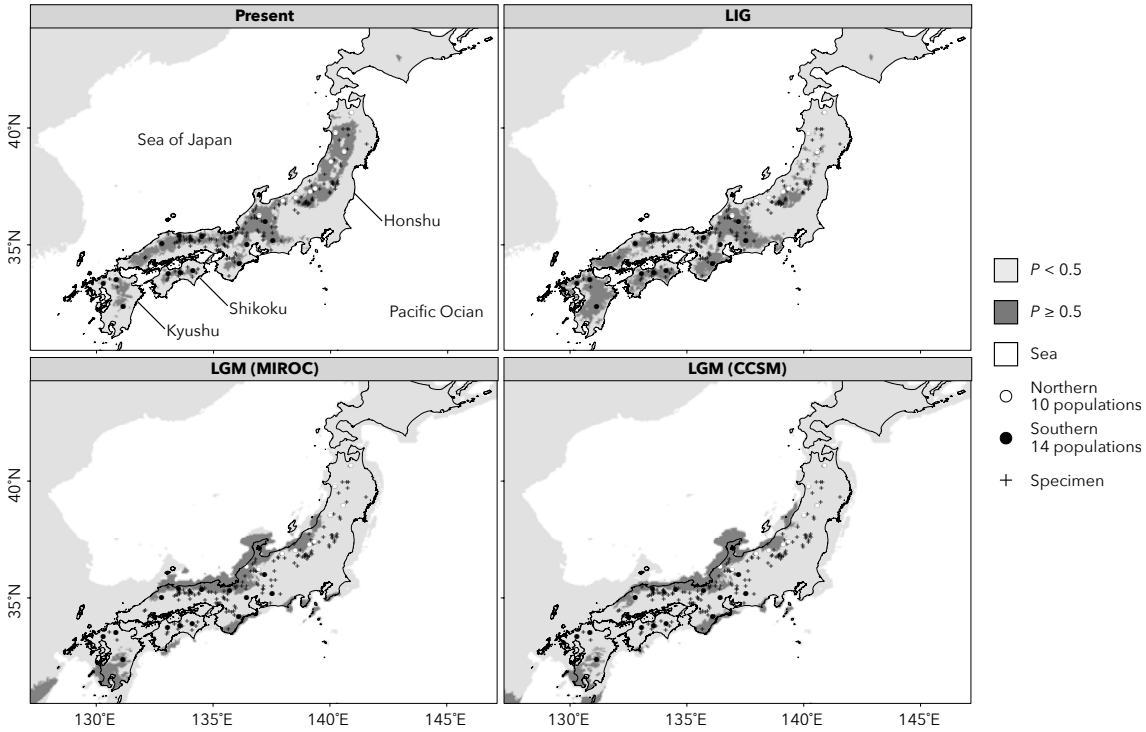
Present
LIG
LGM (MIROC)
LGM (CCSM)
Sea of Japan
Honshu
Shikoku
Kyushu
Pacific Ocian
40°N
35°N
130°E
135°E
140°E
145°E
P < 0.5
P ≥ 0.5
Sea
Northern
10 populations
Southern
14 populations
Specimen

SUPPORTING INFORMATION

Table S1. The four non-coding chloroplast DNA regions that were sequenced in this study

Region	Primer name	Sequence 5′–3′	Length (bp)	T_a (ºC)	Reference
*trn*S–*trn*G	trnS^{GCU}	AGA TAG GGA TTC GAA CCC TCG GT	684	55	Shaw *et al.* (2005)
	5′trnG2S	TTT TAC CAC TAA ACT ATA CCC GC			Shaw *et al.* (2005)
*trn*T–*psb*D	trnT$^{(GGU)}$-R	CCC TTT TAA CTC AGT GGT AG	1461	55	Shaw *et al.* (2007)
	psbD	CTC CGT ARC CAG TCA TCC ATA			Shaw *et al.* (2007)
*trn*T–*trn*L	trnT^{UGU}2F	CAA ATG CGA TGC TCT AAC CT	681	55	Shaw *et al.* (2005)
	b	TCT ACC GAT TTC GCC ATA TC			Taberlet *et al.* (1991)
*rpl*36–*inf*A–*rps*8–*rpl*14	rpL36	GGR TTG GAA CAA ATT ACT ATA ATT CG	1106	55	Shaw *et al.* (2007)
	rpL14	AAG GAA ATC CAA AAG GAA CTC G			Shaw *et al.* (2007)

T_a, annealing temperature.

Table S2. Prior distributions in the population size change models

Parameter	Distribution
N_{CUR}	Log-uniform (10^3, 10^6)
G	Uniform (-0.001, 0)
T	Log-uniform (10^0, 10^5)
N_{ANC}	Log-uniform (10^3, 10^6)
μ for nSSR	Log-uniform (10^{-5}, 10^{-3})
Shape	Uniform (0.5, 5)
P_{GSM}	Uniform (0, 1)

Table S3. Prior distributions in the population divergence models

Parameter	Distribution	Note
N_N	Log-uniform (10^3, 10^6)	
N_S	Log-uniform (10^3, 10^6)	
G		Fixed to -2.24×10^{-4}
T_{DIV}	Log-uniform (10^2, 10^6)	
Nm_{NS}	Log-uniform (10^{-3}, 10^1)	
Nm_{SN}	Log-uniform (10^{-3}, 10^1)	
β	Uniform (0, 1)	
μ for nSSR	Log-uniform (10^{-5}, 10^{-3})	
shape	Uniform (0.5, 5)	
P_{GSM}	Uniform (0, 1)	

Table S4. Genetic diversity at 10 nuclear microsatellite loci across the 24 populations of *Magnolia salicifolia* studied

Locus	*A*	H_S	H_T	F_{ST}	G'_{ST}	*D*
stm0002	23	0.770	0.905	0.151	0.670	0.612
stm0163	22	0.833	0.917	0.096	0.565	0.525
stm0184	25	0.819	0.915	0.108	0.601	0.553
stm0214	27	0.750	0.921	0.198	0.764	0.714
stm0223	25	0.821	0.905	0.085	0.532	0.490
stm0246	44	0.898	0.966	0.077	0.713	0.696
stm0251	21	0.834	0.918	0.091	0.568	0.528
stm0415	25	0.768	0.893	0.148	0.624	0.562
stm0423	51	0.847	0.965	0.117	0.827	0.805
stm0448	15	0.476	0.674	0.301	0.573	0.394
Average / overall	27.8	0.782	0.898	0.133	0.613	0.556

A, number of alleles; H_S, average gene diversity within populations; H_T, gene diversity in the total population; F_{ST}, Weir & Cockerham's F_{ST}; G'_{ST}, Hedrick's standardized G_{ST}; *D*, Jost's *D*.

Table S5. Nucleotide sequence variation among seven haplotypes in four chloroplast DNA regions of *Magnolia salicifolia* and *M. denudata* (outgroup)

		*trn*S–*trn*G (684 bp)		*trn*T–*psb*D (1461 bp)								
Haplotype	*N*	114	452	941	1026	1194	1805	1825	1999	2041	2051	2089
A	25	-	G	G	G	T	T	G	G	G	A	A
B	7	-	•	•	•	•	•	A	•	•	•	•
C	1	-	•	•	•	•	•	A	•	•	•	•
D	2	-	•	•	•	•	•	•	•	•	•	•
E	2	-	•	•	•	C	•	•	•	•	•	•
F	8	-	•	•	T	•	•	•	•	•	•	G
G	6	I_1	•	•	T	•	•	•	•	A	•	G
M. denudata	1	-	A	A	T	•	C	•	A	•	G	G

Table S5. continued

		*trn*T–*trn*L (681 bp)											*rpl*36–*inf*A–*rps*8–*rpl*14 (1106 bp)		
Haplotype	*N*	2161	2172	2173	2265	2296	2300	2357	2408	2636	2653	2743	3249	3276	3854
A	25	A	A	A	I_2	G	G	G	G	T	G	A	A	G	-
B	7	•	•	•	I_2	•	•	•	•	•	•	•	•	•	-
C	1	•	•	C	I_2	•	•	•	•	•	•	•	•	•	-
D	2	•	C	•	I_2	•	•	•	•	•	•	•	•	•	-
E	2	•	•	•	I_2	•	•	•	•	•	•	•	•	•	-
F	8	•	•	•	I_2	•	•	•	•	•	•	•	•	A	-
G	6	C	•	•	I_2	•	•	T	•	•	•	G	•	•	-
M. denudata	1	•	•	•	•	T	T	T	T	C	T	•	G	•	I_3

N, number of individuals; •, the same nucleotide as in haplotype A; -, deletion; I_1, insertion of TTATCTTTCTTTTCTTTATTCTAT; I_2, insertion of CTATAA; I_3, insertion of GAGAA. Gray columns indicate sites variable within *M. salicifolia*.

Table S6. Three principal components (PCs) explaining the variation in leaf shape

Principal component	Eigenvalue ($\times 10^{-3}$)	Contribution (%)	Cumulative contribution (%)
PC1	3.06	48.83	48.83
PC2	1.35	21.51	70.34
PC3	0.98	15.67	86.01
Overall	6.26		

Only PCs contributing more than 5% are shown.

Table S7. Hierarchically estimated variance components for three principal components (PCs) explaining the variation in leaf shape and leaf area

Layer	PC1 (%)		PC2 (%)		PC3 (%)		Area (%)	
Between lineages	42.2	***	0.4	N.S.	19.2	***	45.3	***
Among populations within lineages	13.3	***	1.9	***	10.0	***	8.4	***
Among individuals within populations	18.0	***	3.2	***	16.4	***	16.1	***
Among leaves within individuals	26.6		94.5		54.4		30.2	

Only PCs contributing more than 5% are shown.

N.S., not significant; **, $P < 0.01$; ***, $P < 0.001$.

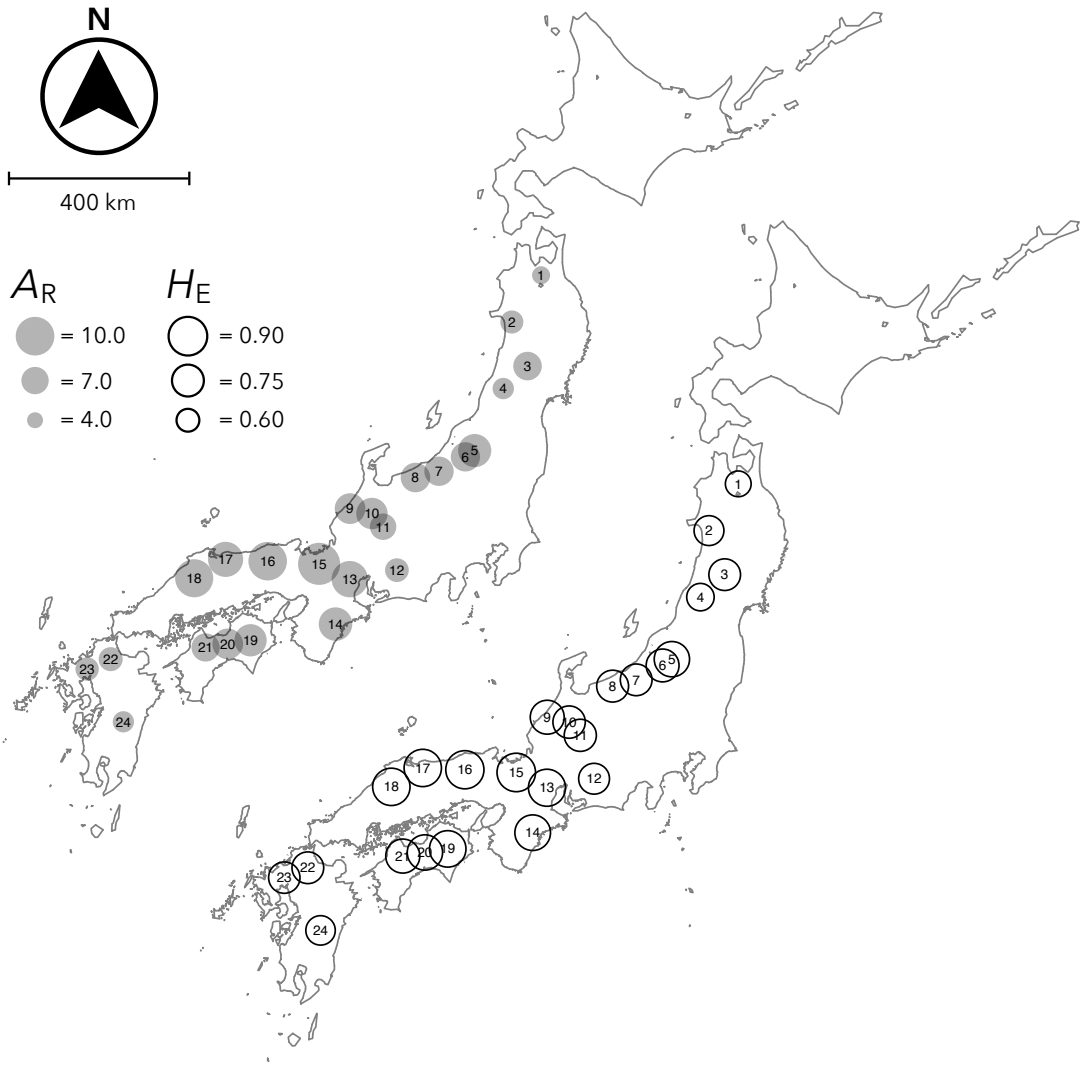

Figure S1. Distributions of genetic diversity in the 24 populations of *Magnolia salicifolia*. A_R and H_E are, respectively, allelic richness based on nine individuals and expected heterozygosity calculated from 10 nuclear microsatellite loci. Numbers indicate the population numbers as listed in Table 1.

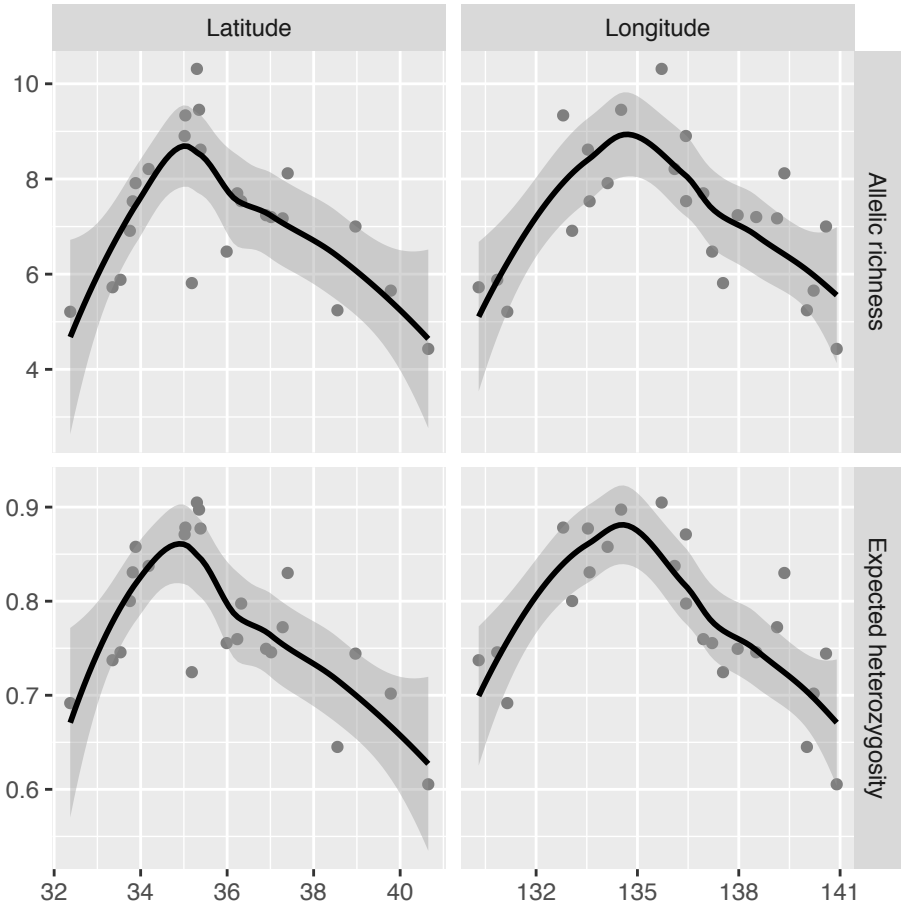

Figure S2. Latitudinal and longitudinal changes in allelic richness based on nine individuals and expected heterozygosity calculated from 10 nuclear microsatellite loci in the 24 populations of *Magnolia salicifolia*. Smoothed lines show to the estimates from locally weighted polynomial regression. Gray areas indicate 95% confidence intervals.

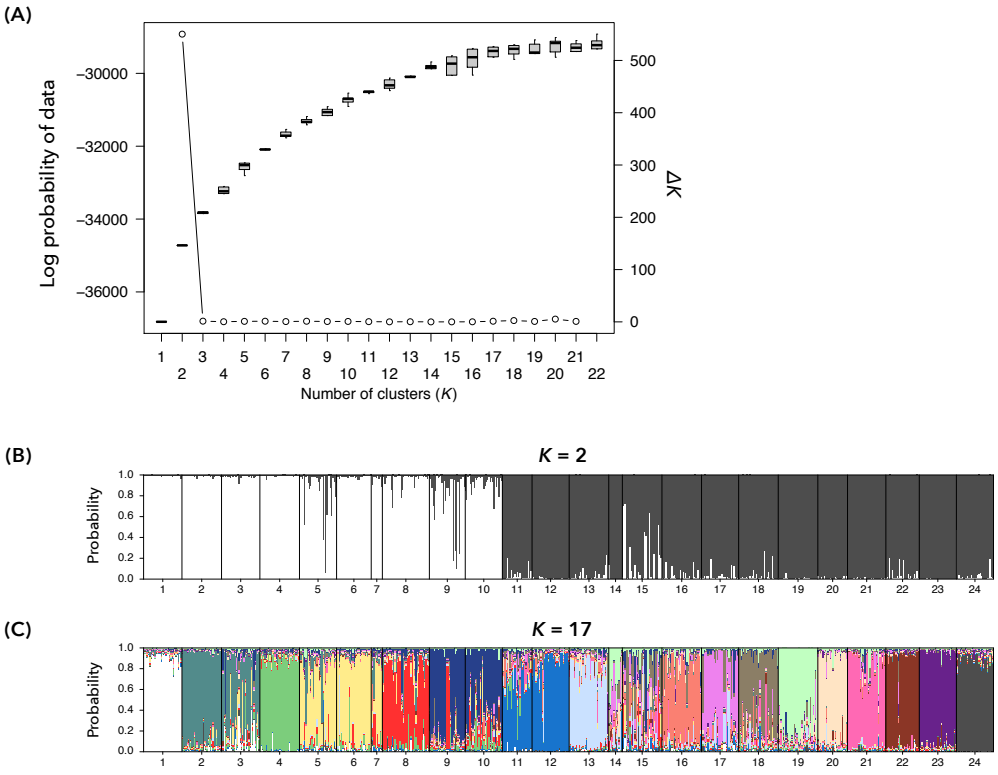

Figure S3. Results from STRUCTURE analysis. Changes in the log probability of data and *ΔK* with increasing *K* (A). Distributions of genetic clusters in each individual at *K* = 2 and 17 (B and C, respectively). Numbers below the bar plots indicate the population numbers listed in Table 1.

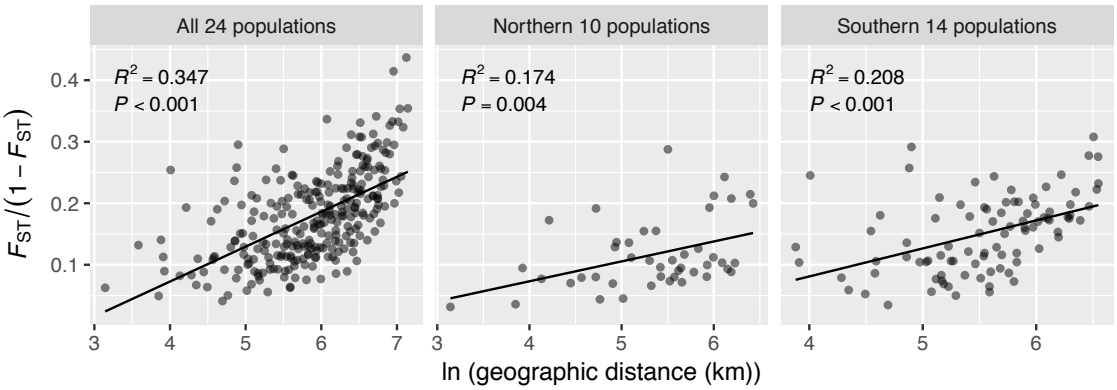

Figure S4. Geographic distance (km) transformed to natural logarithms and genetic distances [$F_{ST}/(1\text{-}F_{ST})$] estimated with 10 nuclear microsatellite loci for all 24, the northern 10 and the southern 14 populations of *Magnolia salicifolia*. *P*-values were calculated by Mantel tests.

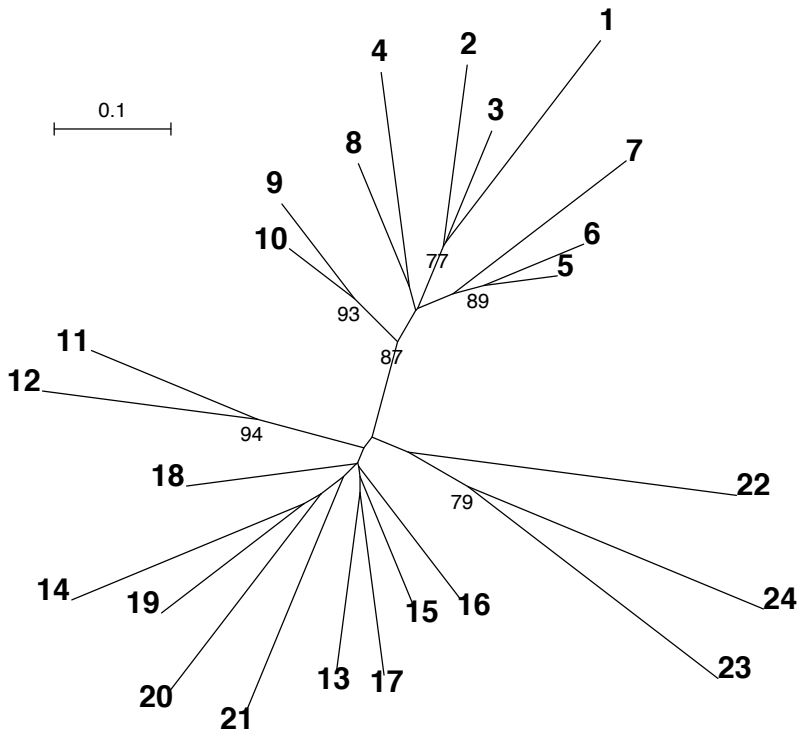

Figure S5. Neighbor-joining tree constructed based on D_A distances estimated with 10 nuclear microsatellite loci among the 24 populations of *Magnolia salicifolia*. Numbers in bold type, and numbers near nodes, indicate the population numbers in Table 1 and the bootstrap probability where > 50%, respectively.

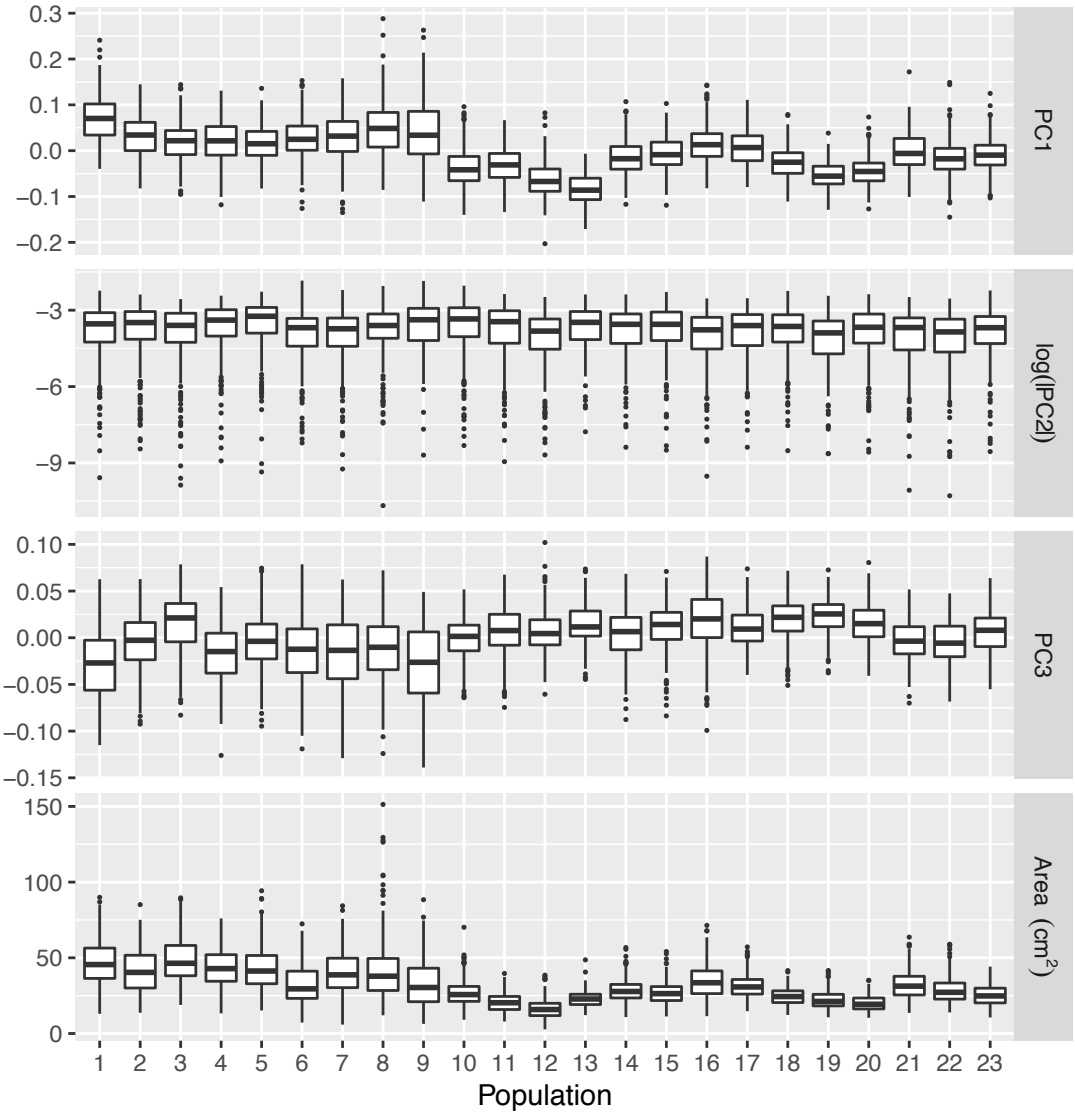

Figure S6. Distributions for PC1, PC2, PC3 and leaf area across 23 populations of *Magnolia salicifolia*.

(A)

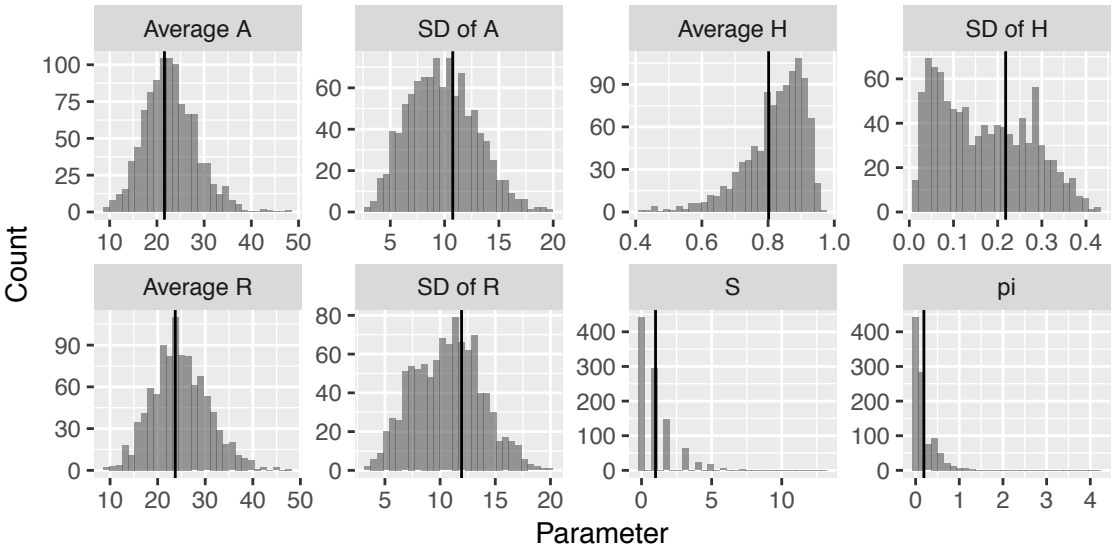

(B)

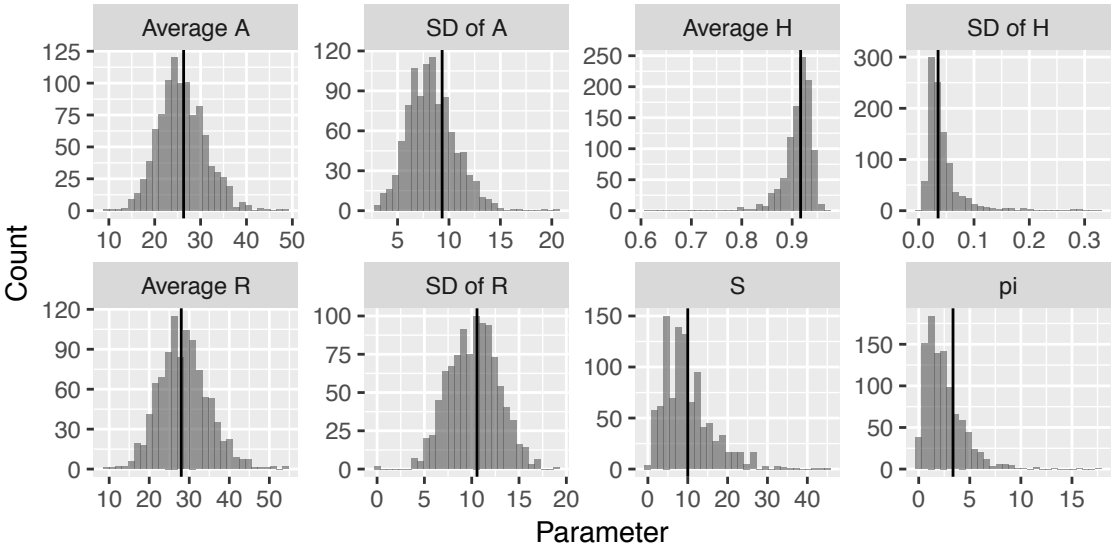

Figure S7. Results from the posterior predictive simulations in models 2 and 1 of the population size change models for the northern (A) and southern (B) lineages of *Magnolia salicifolia*. Histograms and vertical bars indicate predicted and observed values, respectively. *A*, number of alleles; *H*, expected heterozygosity; *R*, allele size range; *S*, number of polymorphic sites; *pi*, mean number of pairwise differences.

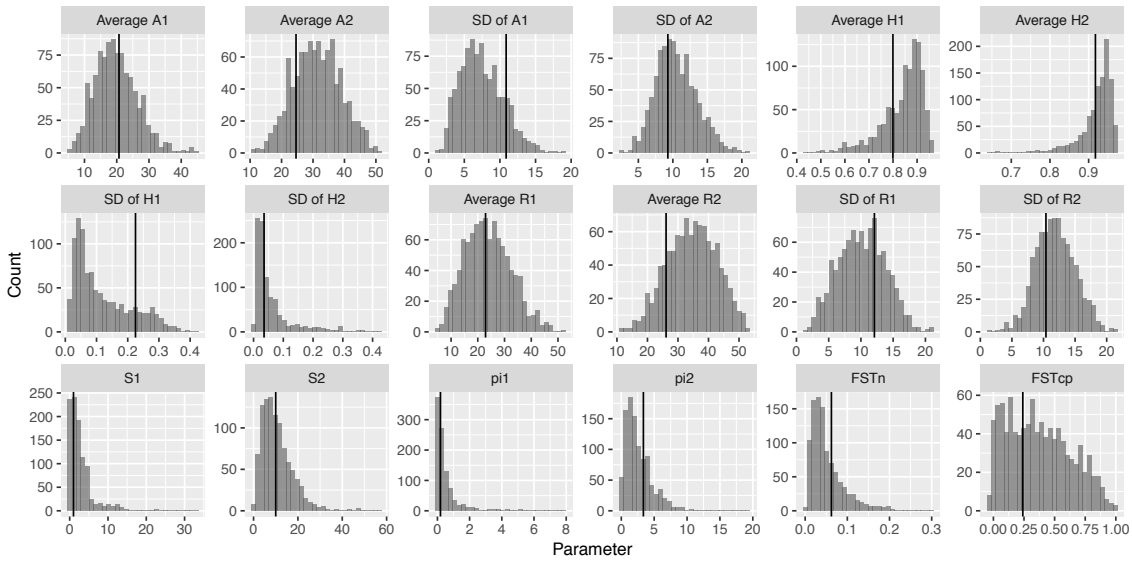

Figure S8. Results from the posterior predictive simulations for the isolation with migration model (IM model) of the population divergence models in the northern and southern lineages of *Magnolia salicifolia*. Histograms and vertical bars indicate predicted and observed values, respectively. *A*, number of alleles; *H*, expected heterozygosity; *R*, allele size range; *S*, number of polymorphic sites; *pi*, mean number of pairwise differences; *FSTn*, F_{ST} over all loci of 10 nuclear microsatellites; *FSTcp*, F_{ST} for chloroplast DNA haplotypes. Plots for the northern and southern lineages are indicated by 1 and 2, respectively.

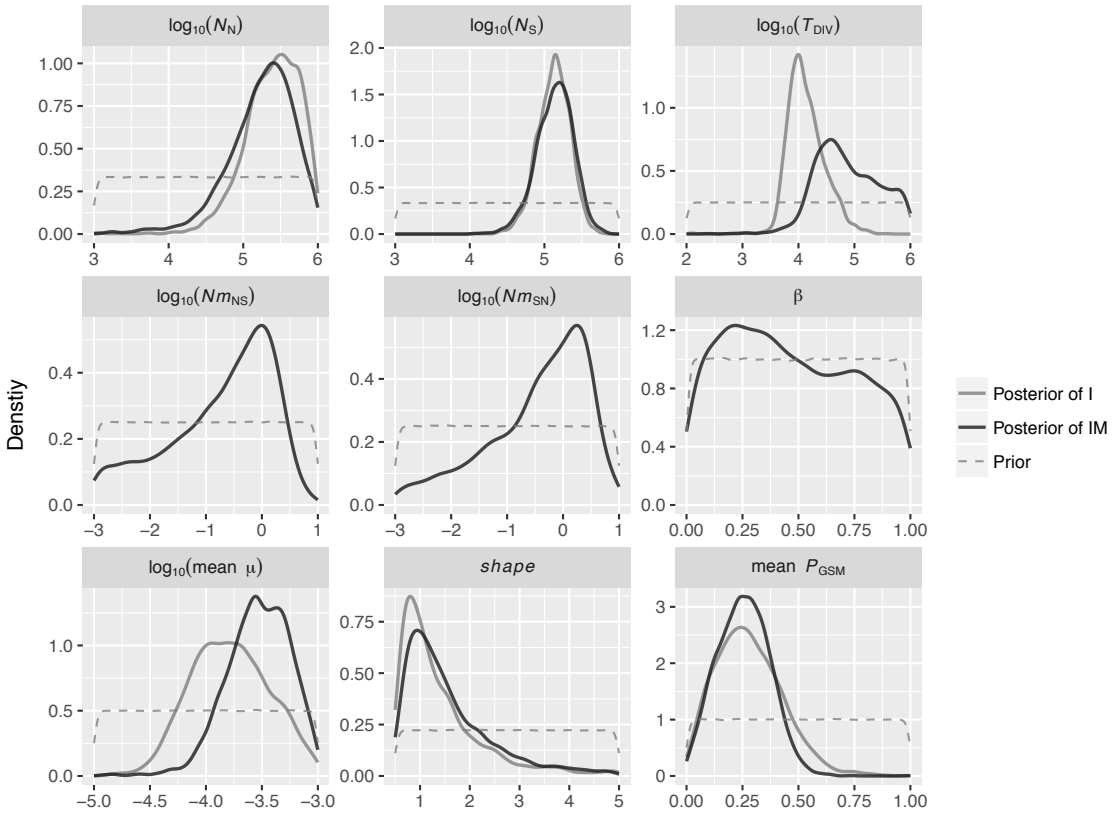

Figure S9. Prior (dashed line) and posterior (solid line) distributions for the isolation (I) model and isolation with migration (IM) models in the northern and southern lineages of *Magnolia salicifolia*.